JOURNAL OF OPTIMIZATION THEORY AND APPLICATIONS: Vol. 57, No. 1, APRIL 1988

# Optimal Penetration Landing Trajectories in the Presence of Windshear[1,2,3]

A. MIELE,[4] T. WANG,[5] H. WANG,[6] AND W. W. MELVIN[7]

**Abstract.** This paper is concerned with optimal flight trajectories in the presence of windshear. The penetration landing problem is considered with reference to flight in a vertical plane, governed by either one control (the angle of attack, if the power setting is predetermined) or two controls (the angle of attack and the power setting). Inequality constraints are imposed on the angle of attack, the power setting, and their time derivatives.

The performance index being minimized measures the deviation of the flight trajectory from a nominal trajectory. In turn, the nominal trajectory includes two parts: the approach part, in which the slope is constant; and the flare part, in which the slope is a linear function of the horizontal distance. In the optimization process, the time is free; the absolute path inclination at touchdown is specified; the touchdown velocity is subject to upper and lower bounds; and the touchdown distance is subject to upper and lower bounds.

Three power setting schemes are investigated: (S1) maximum power setting; (S2) constant power setting; and (S3) control power setting. In Scheme (S1), it is assumed that, immediately after the windshear onset, the power setting is increased at a constant time rate until maximum power setting is reached; afterward, the power setting is held constant; in this scheme, the only control is the angle of attack. In Scheme (S2), it is assumed that the power setting is held at a constant value, equal

[1] Portions of this paper were presented at the AIAA 26th Aerospace Sciences Meeting, Reno, Nevada, January 11–14, 1988 (Paper No. AIAA-88-0580).

[2] This research was supported by NASA-Langley Research Center, Grant No. NAG-1-516, by Boeing Commercial Airplane Company (BCAC), and by Air Line Pilots Association (ALPA).

[3] The authors are indebted to Dr. R. L. Bowles, NASA-Langley Research Center, and to Dr. G. R. Hennig, Boeing Commercial Airplane Company, for helpful discussions.

[4] Professor of Aerospace Sciences and Mathematical Sciences, Aero-Astronautics Group, Rice University, Houston, Texas.

[5] Senior Research Scientist, Aero-Astronautics Group, Rice University, Houston, Texas.

[6] Graduate Student, Aero-Astronautics Group, Rice University, Houston, Texas.

[7] Captain, Delta Airlines, Atlanta, Georgia; and Chairman, Airworthiness and Performance Committee, Air Line Pilots Association (ALPA), Washington, DC.



0022-3239/88/0400-0001$06.00/00 

to the prewindshear value; in this scheme, the only control is the angle of attack. In Scheme (S3), the power setting is regarded as a control, just as the angle of attack.

Under the above conditions, the optimal control problem is solved by means of the primal sequential gradient-restoration algorithm (PSGRA). Numerical results are obtained for several combinations of windshear intensities and initial altitudes. The main conclusions are given below with reference to strong-to-severe windshears.

In Scheme (S1), the touchdown requirements can be satisfied for relatively low initial altitudes, while they cannot be satisfied for relatively high initial altitudes; the major inconvenient is excess of velocity at touchdown. In Scheme (S2), the touchdown requirements cannot be satisfied, regardless of the initial altitude; the major inconvenient is defect of horizontal distance at touchdown.

In Scheme (S3), the touchdown requirements can be satisfied, and the optimal trajectories exhibit the following characteristics: (i) the angle of attack has an initial decrease, which is followed by a gradual, sustained increase; the largest value of the angle of attack is attained near the end of the shear; in the aftershear region, the angle of attack decreases gradually; (ii) initially, the power setting increases rapidly until maximum power setting is reached; then, maximum power setting is maintained in the shear region; in the aftershear region, the power setting decreases gradually; (iii) the relative velocity decreases in the shear region and increases in the aftershear region; the point of minimum velocity occurs at the end of the shear; and (iv) depending on the windshear intensity and the initial altitude, the deviations of the flight trajectory from the nominal trajectory can be considerable in the shear region; however, these deviations become small in the aftershear region, and the optimal flight trajectory recovers the nominal trajectory.

A comparison is shown between the optimal trajectories of Scheme (S3) and the trajectories arising from alternative guidance schemes, such as fixed controls (fixed angle of attack, coupled with fixed power setting) and autoland (angle of attack controlled via path inclination signals, coupled with power setting controlled via velocity signals). The superiority of the optimal trajectories of Scheme (S3) is shown in terms of the ability to meet the path inclination, velocity, and distance requirements at touchdown. Therefore, it is felt that guidance schemes based on the properties of the optimal trajectories of Scheme (S3) should prove to be superior to alternative guidance schemes, such as the fixed control guidance scheme and the autoland guidance scheme.

**Key Words.** Flight mechanics, landing, abort landing, penetration landing, optimal trajectories, optimal control, windshear problems, sequential gradient-restoration algorithm, primal sequential gradient-restoration algorithm.

## 1. Introduction

Low-altitude windshear is a threat to the safety of aircraft in take-off and landing (Ref. 1). Over the past 20 years, some 30 aircraft accidents have been attributed to windshear. The most notorious ones are the crash of PANAM Flight 759 of July 9, 1982 at New Orleans International Airport (Boeing B-727 in take-off, Ref. 2) and the crash of Delta Airlines Flight 191 of August 2, 1985 at Dallas-Fort Worth International Airport (Lockheed L-1011 in landing, Refs. 3-5).

Low-altitude windshear is usually associated with a severe meteorological phenomenon, called the downburst. In turn, a downburst involves a descending column of air, which then spreads horizontally in the neighborhood of the ground. This condition is hazardous, because an aircraft in take-off or landing might encounter a headwind coupled with a downdraft, followed by a tailwind coupled with a downdraft. The transition from headwind to tailwind engenders a transport acceleration, and hence a windshear inertia force (the product of the transport acceleration and the mass of the aircraft). In turn, the windshear inertia force can be as large as the drag of the aircraft, and in some cases as large as the thrust of the engines. Hence, an inadvertent encounter with a low-altitude windshear can be a serious problem for even a highly skilled pilot.

This paper is concerned with the landing problem. When the pilot of an aircraft on a glide path detects an inadvertent encounter with a low-altitude windshear, he has two choices; (i) penetration landing or (ii) abort landing. Clearly, if the initial altitude is high enough, abort landing is a safer procedure than penetration landing; on the other hand, if the initial altitude is low enough, the opposite might be true: in penetration landing, the aircraft might have to traverse only a part of the shear region; in abort landing, the aircraft might have to traverse the whole of the shear region.

When studying the penetration landing problem, one can take two points of view: (a) optimization and (b) guidance. In optimization studies, one assumes that global information on the wind flow field is available and determines the optimal trajectory, namely, the flight trajectory minimizing a suitable performance index, while satisfying the constraining relations. In guidance studies, one assumes that only local information on the wind flow field is available and determines a near-optimal trajectory, namely, a trajectory which approximates the behavior of the optimal trajectory, while utilizing only local information on the state of the aircraft and the wind. Obviously, because of difficulties in securing global information and because of limitation to on-board computer capacity, an optimal trajectory is not implementable in the near future. Nevertheless, the study of an optimal trajectory is important, because it leads to an ideal benchmark that it is

desirable to approach when developing a guidance scheme or a piloting strategy; clearly, this ideal benchmark enables one to evaluate the relative merits of different guidance schemes or piloting strategies.

To sum up, this paper deals with the optimization of penetration landing trajectories. We note that, in this area of problems, previous optimization and guidance studies can be found in Refs. 6–10. We consider flight in a vertical plane, governed by either one control (the angle of attack, if the power setting is predetermined) or two controls (the angle of attack and the power setting). We impose inequality constraints on the angle of attack, the power setting, and their time derivatives. Also, we impose the following touchdown requirements: (i) the absolute path inclination at touchdown is to be $-0.5$ deg; (ii) the velocity at touchdown is to be within 30 knots of the nominal value; and (iii) the horizontal distance at touchdown is to be within 1000 ft of the nominal value. Under these constraints, we determine the control distribution which minimizes a performance index measuring the deviation of the flight trajectory from the nominal trajectory. In turn, the nominal trajectory includes two parts: the approach part, in which the absolute path inclination is constant; and the flare part, in which the absolute path inclination is a linear function of the horizontal distance.

We consider three power setting schemes: (S1) maximum power setting; (S2) constant power setting; and (S3) control power setting.[8] In Scheme (S1), we assume that, immediately after the windshear onset, the power setting is increased at a constant time rate until maximum power setting is reached; afterward, the power setting is held constant; in this scheme, the only control is the angle of attack. In Scheme (S2), we assume that the power setting is held at a constant value, the initial value; in this scheme, the only control is the angle of attack. In Scheme (S3), we regard the power setting as a control, just as the angle of attack. Clearly, the number of independent controls is one in Scheme (S1), one in Scheme (S2), and two in Scheme (S3).

Under the above conditions, we determine optimal penetration landing trajectories for several combinations of windshear intensities and initial altitudes. After concluding that the optimal trajectories of Scheme (S3) are superior to the optimal trajectories of Scheme (S1) and Scheme (S2), we compare the optimal trajectories of Scheme (S3) with alternative guidance trajectories, namely, constant control guidance trajectories and autoland guidance trajectories.[9] In a companion paper (Ref. 11), we develop new

[8] Within the context of this paper, the term "power setting" is employed in the sense of "thrust setting."

[9] Within the context of this paper, the term "autoland" is employed to denote the combination of automatic pilot and automatic throttle.

guidance schemes, based on the properties of the optimal trajectories and approximating the properties of the optimal trajectories.

We close this introduction by noting that the present paper and its companion paper (Ref. 11) are part of a comprehensive research program undertaken at Rice University on optimal trajectories, guidance schemes, and piloting strategies for take-off, abort landing, and penetration landing. For previous studies of optimal trajectories and guidance schemes for take-off and abort landing, see Refs. 12–20 and references therein.

## 2. Notations

Throughout the paper, the following notations are employed:

$C_D$ = drag coefficient;
$C_L$ = lift coefficient;
$D$ = drag force, lb;
$g$ = acceleration of gravity, ft sec$^{-2}$;
$h$ = altitude, ft;
$L$ = lift force, lb;
$m$ = mass, lb ft$^{-1}$ sec$^2$;
$S$ = reference surface, ft$^2$;
$T$ = thrust force, lb;
$V$ = relative velocity, ft sec$^{-1}$;
$V_e$ = absolute velocity, ft sec$^{-1}$;
$W = mg$ = weight, lb;
$W_h$ = $h$-component of wind velocity, ft sec$^{-1}$;
$W_x$ = $x$-component of wind velocity, ft sec$^{-1}$;
$x$ = horizontal distance, ft.

**Greek Symbols**

$\alpha$ = relative angle of attack (wing), rad;
$\alpha_e$ = absolute angle of attack (wing), rad;
$\beta$ = engine power setting;
$\gamma$ = relative path inclination, rad;
$\gamma_e$ = absolute path inclination, rad;
$\delta$ = thrust inclination, rad;
$\theta$ = pitch attitude angle (wing), rad;
$\lambda$ = wind intensity parameter;
$\rho$ = air density, lb ft$^{-4}$ sec$^2$;
$\tau$ = flight time, sec.

## 3. System Description

In this paper, we make use of the relative wind-axes system in connection with the following assumptions: (a) the aircraft is a particle of constant

mass; (b) flight takes place in a vertical plane; (c) Newton's law is valid in an Earth-fixed system; and (d) the wind flow field is steady.

With the above premises, the equations of motion include the kinematical equations

$$\dot{x} = V\cos\gamma + W_x, \tag{1a}$$

$$\dot{h} = V\sin\gamma + W_h, \tag{1b}$$

and the dynamical equations

$$\dot{V} = (T/m)\cos(\alpha+\delta) - D/m - g\sin\gamma - (\dot{W}_x\cos\gamma + \dot{W}_h\sin\gamma), \tag{2a}$$

$$\dot{\gamma} = (T/mV)\sin(\alpha+\delta) + L/mV - (g/V)\cos\gamma + (1/V)(\dot{W}_x\sin\gamma - \dot{W}_h\cos\gamma). \tag{2b}$$

Because of assumption (d), the total derivatives of the wind velocity components and the corresponding partial derivatives satisfy the relations

$$\dot{W}_x = (\partial W_x/\partial x)(V\cos\gamma + W_x) + (\partial W_x/\partial h)(V\sin\gamma + W_h), \tag{3a}$$

$$\dot{W}_h = (\partial W_h/\partial x)(V\cos\gamma + W_x) + (\partial W_h/\partial h)(V\sin\gamma + W_h). \tag{3b}$$

These equations must be supplemented by the functional relations

$$T = T(h, V, \beta), \tag{4a}$$

$$D = D(h, V, \alpha), \qquad L = L(h, V, \alpha), \tag{4b}$$

$$W_x = W_x(x, h), \qquad W_h = W_h(x, h), \tag{4c}$$

and by the analytical relations

$$V_{ex} = V\cos\gamma + W_x, \qquad V_{eh} = V\sin\gamma + W_h, \tag{5a}$$

$$V_e = \sqrt{(V_{ex}^2 + V_{eh}^2)}, \qquad \gamma_e = \arctan(V_{eh}/V_{ex}), \tag{5b}$$

$$\theta = \alpha + \gamma, \qquad \alpha_e = \alpha + \gamma - \gamma_e. \tag{5c}$$

For a given value of the thrust inclination $\delta$, the differential system (1)–(4) involves four state variables [the horizontal distance $x(t)$, the altitude $h(t)$, the velocity $V(t)$, and the relative path inclination $\gamma(t)$] and two control variables [the angle of attack $\alpha(t)$ and the power setting $\beta(t)$]. However, the number of control variables reduces to one (the angle of attack), if the power setting is specified in advance. The quantities defined by the analytical relations (5) can be computed a posteriori, once the values of the state and the control are known.

**3.1. Inequality Constraints.** The angle of attack $\alpha$ and its time derivative $\dot{\alpha}$ are subject to the inequalities

$$\alpha \leq \alpha_*, \tag{6a}$$

$$-\dot{\alpha}_* \leq \dot{\alpha} \leq \dot{\alpha}_*, \tag{6b}$$

where $\alpha_*$ is a prescribed upper bound and $\dot{\alpha}_*$ is prescribed, positive constant.

For the optimal trajectories discussed in Section 4, Ineqs. (6) are enforced indirectly via the following transformation technique:

$$\alpha = \alpha_* - u^2, \tag{7a}$$

$$\dot{u} = -(\dot{\alpha}_*/2u) \sin \phi, \qquad |u| \geq \varepsilon, \tag{7b}$$

$$\dot{u} = -(\dot{\alpha}_*/2u) \sin^2(\pi u/2\varepsilon) \sin \phi, \qquad |u| \leq \varepsilon. \tag{7c}$$

Here, $u(t)$, $\phi(t)$ are auxiliary variables and $\varepsilon$ is a small, positive constant, which is introduced to prevent the occurrence of singularities. Note that the right-hand sides of Eqs. (7b)–(7c) are continuous and have continuous first derivatives at $|u| = \varepsilon$. Clearly, when using Eqs. (7) in conjunction with Eqs. (1)–(4), one must regard $\alpha(t)$, $u(t)$ as state variables and $\phi(t)$ as control variable.

The power setting $\beta$ and its time derivatives $\dot{\beta}$ are subject to the inequalities

$$\beta_* \leq \beta \leq 1, \tag{8a}$$

$$-\dot{\beta}_* \leq \dot{\beta} \leq \dot{\beta}_*, \tag{8b}$$

where $\beta_*$ is a prescribed lower bound and $\dot{\beta}_*$ is a prescribed, positive constant.

For the optimal trajectories discussed in Section 4, Ineqs. (8) are satisfied directly if the power setting distribution $\beta(t)$ is specified in advance. On the other hand, if the power setting distribution $\beta(t)$ is not specified in advance [that is, if $\beta(t)$ is regarded as a control], it is convenient to rewrite Ineqs. (8) in the form

$$\beta \geq \beta_*, \tag{9a}$$

$$\beta \leq 1, \tag{9b}$$

$$-\dot{\beta}_* \leq \dot{\beta} \leq \dot{\beta}_*. \tag{9c}$$

Then, Ineq. (9a) is enforced indirectly via a penalty function technique, while Ineqs. (9b)–(9c) are enforced indirectly via the following transformation technique, which is analogous to (7):

$$\beta = 1 - w^2, \tag{10a}$$

$$\dot{w} = -(\dot{\beta}_*/2w) \sin \psi, \qquad |w| \geq \eta, \tag{10b}$$

$$\dot{w} = -(\dot{\beta}_*/2w) \sin^2(\pi w/2\eta) \sin \psi, \qquad |w| \leq \eta. \tag{10c}$$

Here, $w(t)$, $\psi(t)$ are auxiliary variables and $\eta$ is a small, positive constant, which is introduced to prevent the occurrence of singularities. Note that the right-hand sides of Eqs. (10b)-(10c) are continuous and have continuous first derivatives at $|w| = \eta$. Clearly, when using Eqs. (10) in conjunction with Eqs. (1)-(4), one must regard $\beta(t)$, $w(t)$ as state variables and $\psi(t)$ as control variable.

**3.2. Approximations for the Forces.** Here, we discuss the approximations employed in the description of the forces acting on the aircraft, namely, the thrust, the drag, the lift, and the weight.

**Thrust.** The thrust $T$ is written in the form

$$T = \beta T_*, \tag{11a}$$

$$T_* = A_0 + A_1 V + A_2 V^2, \tag{11b}$$

where $T_*$ is a reference thrust (the thrust corresponding to the power setting $\beta = 1$) and $\beta$ is the power setting.

For the reference thrust, the coefficients $A_0, A_1, A_2$ depend on the altitude of the runway and the ambient temperature. They can be determined with a least-square fit of manufacturer-supplied data over a given interval of velocities. For the power setting, see the discussion below.

*Scheme (S1).* For the maximum power setting scheme, we recall the basic assumption, namely: immediately after the windshear onset, the power setting is increased at a constant time rate until maximum power setting is reached; afterward, the power setting is held constant. This yields the relations

$$\beta = \beta_0 + \dot{\beta}_0 t, \qquad 0 \le t \le \sigma, \tag{12a}$$

$$\beta = 1, \qquad \sigma \le t \le \tau, \tag{12b}$$

where

$$\sigma = (1 - \beta_0)/\dot{\beta}_0. \tag{12c}$$

Here, $\beta_0$ is the initial power setting, $\dot{\beta}_0$ is the constant rate of increase of the power setting, $\sigma$ is the time at which maximum power setting is reached, and $\tau$ is the final time.

*Scheme (S2).* For the constant power setting scheme, we recall the basic assumption, namely: the power setting is held at a constant value, the initial value. This yields the relation

$$\beta = \beta_0, \qquad 0 \le t \le \tau, \tag{13}$$

where $\beta_0$ is the initial power setting.

*Scheme (S3).* For the control power setting scheme, we regard $\beta(t)$ as a control, subject to Ineqs. (8), which are equivalent to Ineqs. (9). In turn, Ineq. (9a) is enforced indirectly via a penalty function technique, while Ineqs. (9b)–(9c) are forced indirectly via the transformation technique (10), rewritten here for convenience:

$$\beta = 1 - w^2, \tag{14a}$$

$$\dot{w} = -(\dot{\beta}_*/2w)\sin\psi, \qquad |w| \geq \eta, \tag{14b}$$

$$\dot{w} = -(\dot{\beta}_*/2w)\sin^2(\pi w/2\eta)\sin\psi, \qquad |w| \leq \eta. \tag{14c}$$

When using Eqs. (14) in conjunction with Eqs. (1)–(4), we must regard $\beta(t)$, $w(t)$ as state variables and $\psi(t)$ as control variable.

**Drag.** The drag $D$ is written in the form

$$D = (1/2)C_D\rho SV^2, \tag{15a}$$

$$C_D = B_0 + B_1\alpha + B_2\alpha^2, \qquad \alpha \leq \alpha_*, \tag{15b}$$

where $\rho$ is the air density (assumed constant), $S$ is a reference surface, $V$ is the relative velocity, and $C_D$ is the drag coefficient. The coefficients $B_0$, $B_1$, $B_2$ depend on the flap setting and the undercarriage position (gear up or gear down); they can be determined with a least-square fit of manufacturer-supplied data over the interval $0 \leq \alpha \leq \alpha_*$.

**Lift.** The lift $L$ is written in the form

$$L = (1/2)C_L\rho SV^2, \tag{16a}$$

$$C_L = C_0 + C_1\alpha, \qquad \alpha \leq \alpha_{**}, \tag{16b}$$

$$C_L = C_0 + C_1\alpha + C_2(\alpha - \alpha_{**})^2, \qquad \alpha_{**} \leq \alpha \leq \alpha_*, \tag{16c}$$

where $\rho$ is the air density (assumed constant), $S$ is a reference surface, $V$ is the relative velocity, and $C_L$ is the lift coefficient. The coefficients $C_0$, $C_1$, $C_2$ depend on the flap setting and the undercarriage position (gear up or gear down); they can be determined with a least-square fit of manufacturer-supplied data over the intervals $0 \leq \alpha \leq \alpha_{**}$ and $\alpha_{**} \leq \alpha \leq \alpha_*$.

**Weight.** The mass $m$ is regarded to be constant. Hence, the weight $W = mg$ is regarded to be constant.

**Remark.** The coefficients $A_i$, $B_i$, $C_i$, $i = 0, 1, 2$, appearing in Eqs. (11), (15), (16), can be determined with a least-square fit of manufacturer-supplied data. Numerical experiments show that the resulting precision in the thrust function $T_*(V)$, drag coefficient function $C_D(\alpha)$, and lift coefficient function

$C_L(\alpha)$ is of order 1% or better in the range of velocities and angles of attack having interest in a windshear encounter. These functions are plotted in Fig. 1 with reference to the Boeing B-727 aircraft powered by three JT8D-17 turbofan engines.

**3.3. Approximations for the Windshear.** The representation of the flow field characteristic of a downburst (Refs. 21-22) is usually done in one of two ways: (i) by solving numerically the basic fluid mechanics equations and associated boundary conditions; (ii) by employing simple analytical approximations, suggested by the analysis of aircraft accidents. For optimization and guidance studies, the disadvantage of (i) lies in excessive CPU time and excessive memory requirements; on the other hand, the disadvantage of (ii) lies in the possible dissatisfaction of the basic fluid mechanics equations and limited accuracy.

In the light of (i) and (ii), an alternative point of view is taken in this paper: (iii) the flow field characteristic of a downburst is represented by solving numerically the basic fluid mechanics equations and associated boundary conditions and then developing analytical approximations to the numerical solutions. This point of view leads to the folllowing windshear model, valid for $h \leq 1000$ ft (see Fig. 2):

$$W_x = \lambda A(x), \tag{17a}$$

$$W_h = \lambda (h/h_*) B(x), \tag{17b}$$

with the implication that (see Table 1)

$$\Delta W_x = 100\lambda, \tag{17c}$$

$$\Delta W_h = 50\lambda (h/h_*). \tag{17d}$$

Here, the parameter $\lambda$ characterizes the intensity of the windshear/downdraft combination; the function $A(x)$ represents the distribution of the horizontal wind versus the horizontal distance; the function $B(x)$ represents the distribution of the vertical wind versus the horizontal distance; and $h_*$ is a reference altitude, $h_* = 1000$ ft. Also, $\Delta W_x$ is the horizontal wind velocity difference (maximum tailwind minus maximum headwind) and $\Delta W_h$ is the vertical wind velocity difference (maximum updraft minus maximum downdraft).

Concerning the horizontal wind (17a), the function $A(x)$ represents a linear transition from a uniform headwind of $-50$ ft sec$^{-1}$ to a uniform tailwind of $+50$ ft sec$^{-1}$; hence, the wind velocity difference is $\Delta W_x = 100$ ft sec$^{-1}$ if $\lambda = 1$. The transition takes place over a distance $\Delta x = 4600$ ft, starting at $x = 0$ ft and ending at $x = 4600$ ft; the average wind gradient over the horizontal distance interval $300 \leq x \leq 4300$ ft is $\Delta W_x/\Delta x \cong 0.025$ sec$^{-1}$ if $\lambda = 1$.

Concerning the vertical wind (17b), the function $B(x)$ has a bell-shaped form; in particular, the downdraft vanishes at $x = 0$ ft and $x = 4600$ ft and achieves maximum negative value at $x = 2300$ ft; this maximum negative value is $-50\,\text{ft sec}^{-1}$ if $h = 1000$ ft and $\lambda = 1$; hence, $\Delta W_h = 50\text{ft sec}^{-1}$ if $h = 1000$ ft and $\lambda = 1$.

To sum up, the windshear model (17) has the following properties: (a) it represents the transition from a headwind to a tailwind, with nearly constant shear in the core of the downburst; (b) the downdraft achieves maximum negative value at the center of the downburst; (c) the downdraft vanishes at $h = 0$; and (d) the functions $W_x$, $W_h$ nearly satisfy the continuity equation and the irrotationality condition in the core of the downburst.

**3.4. Aircraft Data.** The numerical examples of the subsequent sections refer to a Boeing B-727 aircraft powered by three JT8D-17 turbofan engines. It is assumed that: the aircraft is in quasi-steady flight on a glide slope with inclination $\gamma_e = -3.0$ deg; the runway is located at sea-level altitude; the ambient temperature is 100 deg Fahrenheit; the gear is down; the flap setting is $\delta_F = 30$ deg; the landing weight is $W = 150{,}000$ lb.

The inequality constraints on the angle of attack (6) are enforced with

$$\alpha_* = 17.2 \text{ deg} = 0.3002 \text{ rad}, \tag{18a}$$

$$\dot{\alpha}_* = 3.0 \text{ deg sec}^{-1} = 0.5236E-01 \text{ rad sec}^{-1}. \tag{18b}$$

The inequality constraints on the power setting (9) are enforced with

$$\beta_* = 0.20, \tag{19a}$$

$$\dot{\beta}_* = 0.30 \text{ sec}^{-1}. \tag{19b}$$

**Initial State.** The following initial conditions are assumed:

$$x_0 = 0 \text{ ft}, \tag{20a}$$

$$h_0 = 200,\ 600,\ 1000 \text{ ft}, \tag{20b}$$

$$V_0 = 142 \text{ knots} = 239.7 \text{ ft sec}^{-1}, \tag{20c}$$

$$\gamma_{e0} = -3.0 \text{ deg} = -0.5236E\text{-}01 \text{ rad}. \tag{20d}$$

For the wind model of Section 3.3 and $\lambda = 1.20$, the values (20) imply that

$$\gamma_0 = -2.249 \text{ deg} = -0.3925E\text{-}01 \text{ rad}, \tag{21a}$$

$$\alpha_0 = \ 7.349 \text{ deg} = \ 0.1283 \text{ rad}, \tag{21b}$$

$$\theta_0 = \ 5.100 \text{ deg} = \ 0.8901E\text{-}01 \text{ rad}, \tag{21c}$$

$$\beta_0 = \ 0.3825. \tag{21d}$$

For other values of $\lambda$, see Table 1.

We note that the initial velocity (20c) is FAA certification velocity $V_{\text{ref}}$ augmented by 10 knots ($V_0 = V_{\text{ref}} + 10$ knots). We also note that the values (21) are a consequence of the values (20) and the assumption of quasi-steady flight prior to the windshear onset.

**Final Time.** The final $\tau$ is free. It is to be determined indirectly through the satisfaction of the final condition (22a), given below.

**Final State.** Concerning the altitude and the absolute path inclination at touchdown, the following final values are assumed:

$$h_\tau = 0, \tag{22a}$$

$$\gamma_{e\tau} = -0.5 \text{ deg}. \tag{22b}$$

The value (22b) is a compromise between the need for passenger comfort and the need for avoiding an excessively long flare distance.

Concerning the velocity and the distance at touchdown, it is assumed that the following inequalities must be satisfied:

$$V_{\tau l} \leq V_\tau \leq V_{\tau u}, \tag{23a}$$

$$x_{\tau l} \leq x_\tau \leq x_{\tau u}, \tag{23b}$$

where $V_{\tau l}$, $V_{\tau u}$ denote bounds for the touchdown velocity and $x_{\tau l}$, $x_{\tau u}$ denote bounds for the touchdown distance. These inequalities are converted into equalities via the following trigonometric transformations:

$$V_\tau = (V_{\tau l} + V_{\tau u})/2 + [(V_{\tau u} - V_{\tau l})/2] \sin p, \tag{24a}$$

$$x_\tau = (x_{\tau l} + x_{\tau u})/2 + [(x_{\tau u} - x_{\tau l})/2] \sin q, \tag{24b}$$

where $p$, $q$ denote parameters to be determined together with the flight time $\tau$. In Eqs. (24), the quantities

$$\tilde{V}_\tau = (V_{\tau l} + V_{\tau u})/2, \tag{25a}$$

$$\tilde{x}_\tau = (x_{\tau l} + x_{\tau u})/2 \tag{25b}$$

can be regarded as the nominal values for the velocity and the distance at touchdown.

The velocity bounds in (23)-(25) are given by

$$V_{\tau l} = V_{\text{ref}} - 20 \text{ knots} = V_0 - 30 \text{ knots} = 112.0 \text{ knots} = 189.0 \text{ ft sec}^{-1}, \tag{26a}$$

$$V_{\tau u} = V_{\text{ref}} + 40 \text{ knots} = V_0 + 30 \text{ knots} = 172.0 \text{ knots} = 290.3 \text{ ft sec}^{-1}. \tag{26b}$$

Hence, the nominal velocity at touchdown is given by

$$\tilde{V}_\tau = V_{\text{ref}} + 10 \text{ knots} = V_0 = 142.0 \text{ knots} = 239.7 \text{ ft sec}^{-1}. \tag{26c}$$

The lower bound (26a) is determined by the fact that, if the velocity is too low, it is difficult to control the trajectory in such a way that the touchdown path inclination requirement (22b) can be met. The upper bound (26b) is determined by the need for containing the runway length needed for depleting the velocity to zero after touchdown.

The distance bounds in (23)-(25) are given by

$$x_{\tau l} = \tilde{x}_\tau - 1000 \text{ ft}, \tag{27a}$$

$$x_{\tau u} = \tilde{x}_\tau + 1000 \text{ ft}, \tag{27b}$$

where $\tilde{x}_\tau$ is the nominal distance at touchdown. The bounds (27) are determined by the need of avoiding excessive undershooting/overshooting of the nominal touchdown distance. In turn, the nominal touchdown distance is given by [see (29d)]

$$\tilde{x}_\tau = (h_f - h_0)/\tan \gamma_{e0} - 2h_f/(\tan \gamma_{e0} + \tan \gamma_{e\tau}), \tag{27c}$$

where $\gamma_{e0}$ is the absolute path inclination at the initial point, $\gamma_{e\tau}$ is the absolute path inclination at touchdown, $h_0$ is the initial altitude, and $h_f$ is the altitude at the end of the approach path/beginning of the flare path. The values of the nominal touchdown distance (27c) are given in Table 2 under the assumption that

$$h_f = 50 \text{ ft}, \qquad \gamma_{e0} = -3.0 \text{ deg}, \qquad \gamma_{e\tau} = -0.5 \text{ deg}. \tag{27d}$$

Clearly, for given values of $h_f$, $\gamma_{e0}$, $\gamma_{e\tau}$, the nominal touchdown distance is a linear function of the initial altitude.

**3.5. Nominal Trajectory.** In the absence of windshear, the geometry of a nominal penetration landing trajectory can be computed, based on simple assumptions on the distribution of slopes. Let the nominal glide path be subdivided into an approach path and a flare path. Assume that the slope of the approach path is constant and the slope of the flare path is a linear function of the horizontal distance; namely, assume that

$$dh/dx = \tan \gamma_{e0}, \qquad 0 \le x \le x_f, \tag{28a}$$

$$dh/dx = \tan \gamma_{e0} + [(x - x_f)/(x_\tau - x_f)](\tan \gamma_{e\tau} - \tan \gamma_{e0}), \qquad x_f \le x \le x_\tau. \tag{28b}$$

Upon integration, Eqs. (28) yield the relations

$$h - h_0 = x \tan \gamma_{e0}, \qquad 0 \le x \le x_f, \tag{29a}$$

$$h - h_f = (x - x_f) \tan \gamma_{e0} + [(x - x_f)^2/2(x_\tau - x_f)] \times (\tan \gamma_{e\tau} - \tan \gamma_{e0}), \qquad x_f \le x \le x_\tau, \tag{29b}$$

in which the constants $x_f$, $x_\tau$ are given by

$$x_f = (h_f - h_0)/\tan \gamma_{e0}, \tag{29c}$$

$$x_\tau = (h_f - h_0)/\tan \gamma_{e0} - 2h_f/(\tan \gamma_{e0} + \tan \gamma_{e\tau}). \tag{29d}$$

Equations (29) represent the geometry of the nominal penetration landing trajectory.

## 4. Optimal Flight Trajectories

We refer to penetration landing and we assume that: global information on the wind field is available, that is, the functions $W_x(x, h)$, $W_h(x, h)$ are known in advance; the angle of attack $\alpha(t)$ is subject to Ineqs. (6); and the power setting $\beta(t)$ is subject to Ineqs. (8) or (9). Depending on the power setting scheme employed, three optimal control problems can be formulated: Problem (P1) corresponds to Scheme (S1); Problem (P2) corresponds to Scheme (S2); and Problem (S3) corresponds to Scheme (S3).

**4.1. Problem (P1).** This optimization problem is associated with the maximum power setting scheme [Scheme (S1)]. In this scheme, the function $\beta(t)$ is supplied by Eqs. (12). The feasibility relations include: the state equations (1)–(4); the angle of attack inequality constraints (6), converted into equality constraints by means of the transformations (7); the initial conditions (20); and the final conditions (22). In this system, the state variables are $x(t)$, $h(t)$, $V(t)$, $\gamma(t)$, $\alpha(t)$, $u(t)$; the control variable is $\phi(t)$; and the parameter is $\tau$. With this understanding, we formulate the following Bolza problem: Subject to the previous constraints, minimize the functional

$$I = (1/\tau h_*^2) \int_0^\tau [h - \tilde{h}(x)]^2 \, dt + (K_{v\tau}/V_*^2)(V_\tau - \tilde{V}_\tau)^2 + (K_{x\tau}/x_*^2)(x_\tau - \tilde{x}_\tau)^2. \tag{30}$$

Here, $\tau$ is the flight time; $h_*$ is a reference altitude, $h_* = 1000$ ft; $x_*$ is a reference distance, $x_* = 1000$ ft; $V_*$ is a reference velocity, $V_* = V_0$; $h$ is the instantaneous altitude; $\tilde{h}(x)$ is the nominal altitude [Eqs. (29a)–(29b)]; $V_\tau$ is the touchdown velocity; $\tilde{V}_\tau$ is the nominal touchdown velocity [Eq. (26c)]; $x_\tau$ is the touchdown distance; $\tilde{x}_\tau$ is the nominal touchdown distance [Eq. (27c)]; and $K_{v\tau}$, $K_{x\tau}$ are penalty coefficients, having the following values:

$$K_{v\tau} = 0.002, \tag{31a}$$

$$K_{x\tau} = 0.002. \tag{31b}$$

Note that the functional (30) is the sum of three quadratic terms: the first term measures the deviation of the flight trajectory from the nominal

trajectory; the second term is a penalization term, measuring the deviation of the touchdown velocity from the nominal value; and the third term is a penalization term, measuring the deviation of the touchdown distance from the nominal value. Also note that, in Problem (P1), the trigonometric transformations (24) are bypassed; approximate compliance with the touchdown inequality constraints (23) is enforced via the quadratic penalization terms in the performance index (30).

**4.2. Problem (P2).** This optimization problem is associated with the constant power setting scheme [Scheme (S2)]. In this scheme, the function $\beta(t)$ is supplied by Eq. (13). The feasibility relations include: the state equations (1)-(4); the angle of attack inequality constraints (6), converted into equality constraints by means of the transformations (7); the initial conditions (20); and the final conditions (22). In this system, the state variables are $x(t)$, $h(t)$, $V(t)$, $\gamma(t)$, $\alpha(t)$, $u(t)$; the control variable is $\phi(t)$; and the parameter is $\tau$. With this understanding, we formulate the following Bolza problem: Subject to the previous constraints, minimize the functional

$$I = (1/\tau h_*^2) \int_0^\tau [h - \tilde{h}(x)]^2 \, dt + (K_{v\tau}/V_*^2)(V_\tau - \tilde{V}_\tau)^2$$

$$+ (K_{x\tau}/x_*^2)(x_\tau - \tilde{x}_\tau)^2 - (1/\tau h_*^3) \int_0^\tau K_{ht} h^3 \, dt. \tag{32}$$

Here, $\tau$ is the flight time; $h$ is the instantaneous altitude; $\tilde{h}(x)$ is the nominal altitude [Eqs. (29a)-(29b)]; $V_\tau$ is the touchdown velocity; $\tilde{V}_\tau$ is the nominal touchdown velocity [Eq. (26c)]; $x_\tau$ is the touchdown distance; $\tilde{x}_\tau$ is the nominal touchdown distance [Eq. (27c)]; and $K_{v\tau}$, $K_{x\tau}$, $K_{ht}$ are penalty coefficients, having the following values:

$$K_{v\tau} = 0.0002, \tag{33a}$$

$$K_{x\tau} = 0.0002, \tag{33b}$$

$$K_{ht} = 0, \qquad \text{if } h \geq 0, \tag{33c}$$

$$K_{ht} = 100, \qquad \text{if } h < 0. \tag{33d}$$

Note that the functional (32) is the sum of three quadratic terms and one cubic term; the quadratic terms are the same as in the functional (30); the cubic term is a penalization term, whose function is to ensure that $h \geq 0$ throughout the computation. Also note that, on the boundary $h = 0$, the cubic integrand in (32) is continuous, together with its first derivatives and its second derivatives. Finally note that, in Problem (P2), the trigonometric transformations (24) are bypassed; approximate compliance with the touchdown inequality constraints (23) is enforced via the quadratic penalization terms in the performance index (32).

**4.3. Problem (P3).** This optimization problem is associated with the control power setting scheme [Scheme (S3)]. In this scheme, the function $\beta(t)$ is described by Eqs. (14). The feasiblity relations include: the state equations (1)–(4); the angle of attack inequality constraints (6), converted into equality constraints by means of the transformations (7); the power setting inequality constraints (9b)–(9c), converted into equality constraints by means of the transformations (14); the initial conditions (20); the final conditions (22); and the inequalities (23), converted into equalities by means of the trigonometric transformations (24). In this system, the state variables are $x(t)$, $h(t)$, $V(t)$, $\gamma(t)$, $\alpha(t)$, $u(t)$, $\beta(t)$, $w(t)$; the control variables are $\phi(t)$, $\psi(t)$; and the parameters are $\tau$, $p$, $q$. With this understanding, we formulate the following Bolza problem: Subject to the previous constraints, minimize the functional

$$I=(1/\tau h_*^2)\int_0^\tau [h-\tilde{h}(x)]^2\,dt-(1/\tau)\int_0^\tau K_{\beta t}(\beta-C\beta_*)^3\,dt$$
$$-(1/\tau V_*^3)\int_0^\tau K_{vt}(V_0-V)^3\,dt. \tag{34}$$

Here, $\tau$ is the flight time; $h$ is the instantantaneous altitude; $\tilde{h}(x)$ is the nominal altitude [Eqs. (29a)–(29b)]; $\beta$ is the instantaneous power setting; $\beta_*$ is minimum power setting; $V$ is the instantaneous velocity; $V_0$ is the initial velocity; and $K_{\beta t}$, $K_{vt}$ are penalty coefficients, having the following values:

$$K_{\beta t}=0, \quad \text{if } \beta-C\beta_*\geq 0, \quad C=1.5, \tag{35a}$$
$$K_{\beta t}=100, \quad \text{if } \beta-C\beta_*<0, \quad C=1.5, \tag{35b}$$
$$K_{vt}=0, \quad \text{if } V_0-V\geq 0, \tag{35c}$$
$$K_{vt}=1, \quad \text{if } V_0-V<0. \tag{35d}$$

Note that the functional (34) is the sum of a quadratic term and two cubic terms; the quadratic term measures the deviation of the flight trajectory from the nominal trajectory; the first cubic term is a penalization term, whose function is the avoidance of undershooting of the lower bound for the power setting; and the second cubic term is a penalization term, whose function is the avoidance of overshooting of the initial velocity. Also note that, on the boundaries $\beta=C\beta_*$ and $V=V_0$, the cubic integrands in (34) are continuous together with their first derivatives and their second derivatives. Finally note that the quadratic penalization terms, present in the functionals (30) and (32), are absent from the functional (34); this is due to the fact that, in Problem (P3), the trigonometric transformations (24) are accounted for; compliance with the touchdown inequality constraints (23) is rigorously enforced; hence, the quadratic penalization terms, essential for the functionals (30) and (32), are irrelevant for the functional (34).

**4.4. Sequential Gradient-Restoration Algorithm.** Problems (P1), (P2), (P3) are Bolza problems of optimal control. They can be solved using the family of sequential gradient-restoriation algorithms for optimal control problems (SGRA, Refs. 23–24) in either the primal formulation (PSGRA) or the dual formulation (DSGRA).

Regardless of whether the primal formulation is used or the dual formulation is used, sequential gradient-restoration algorithms involve a sequence of two-phase cycles, each cycle including a gradient phase and a restoration phase. In the gradient phase, the value of the augmented functional is decreased, while avoiding excessive constraint violation. In the restoration phase, the value of the constraint error is decreased, while avoiding excessive change in the value of the functional. In a complete gradient-restoration cycle, the value of the functional is decreased, while the constraints are satisfied to a preselected degree of accuracy. Thus, a succession of suboptimal solutions is generated, each new solution being an improvement over the previous one from the point of view of the value of the functional being minimized.

The convergence conditions are represented by the relations

$$P \leq \varepsilon_1, \qquad Q \leq \varepsilon_2. \tag{36}$$

Here, $P$ is the norm squared of the error in the constraints; $Q$ is the norm squared of the error in the optimality conditions; and $\varepsilon_1$, $\varepsilon_2$ are preselected, small, positive numbers.

In this work, the sequential gradient-restoration algorithm is employed in conjunction with the primal formulation (PSGRA). The algorithmic details can be found in Refs. 23–24; they are omitted here, for the sake of brevity.

## 5. Numerical Results for Optimal Flight Trajectories

Problems (P1), (P2), (P3) were solved with the sequential gradient-restoration algorithm, employed in conjunction with the primal formulation (PSGRA, Refs. 23–24). Computations were performed at Rice University using an NAS-AS-9000 computer. Several combinations of an initial altitudes and windshear intensities were considered, specifically:

$$h_0 = 200, 600, 1000 \text{ ft}, \tag{37a}$$

$$\Delta W_x = 100, 120, 140 \text{ ft sec}^{-1}. \tag{37b}$$

The numerical results are shown in Tables 3–5 and Figs. 3–5.

Table 3 refers to Problem (P1); Table 4 refers to Problem (P2); and Table 5 refers to Problem (P3). Each table exhibits the following information: the final time $\tau$, the touchdown absolute path inclination $\gamma_{e\tau}$, the touchdown miss velocity $V_\tau - \tilde{V}_\tau$, the touchdown miss distance $x_\tau - \tilde{x}_\tau$, the maximum deviation from the nominal trajectory,

$$|\Delta h|_{\max} = \max_t |h - \tilde{h}(x)|, \tag{38a}$$

and the average deviation from the nominal trajectory,

$$|\Delta h|_{\text{ave}} = \sqrt{\left\{(1/\tau)\int_0^\tau [h - \tilde{h}(x)]^2\, dt\right\}}. \tag{38b}$$

Figure 3 refers to $h_0 = 200$ ft and $\Delta W_x = 120$ ft sec$^{-1}$; Fig. 4 refers to $h_0 = 600$ ft and $\Delta W_x = 120$ ft sec$^{-1}$; and Fig. 5 refers to $h_0 = 1000$ ft and $\Delta W_x = 120$ ft sec$^{-1}$. The following trajectories are shown in Figs. 3–5: the optimal trajectory for maximum power setting (OT1); the optimal trajectory for constant power setting (OT2); the optimal trajectory for control power setting (OT3); and the nominal trajectory (NT). Each figure includes four parts: the altitude $h$ versus the distance $x$; the relative velocity $V$ versus the distance $x$; the angle of attack $\alpha$ versus the distance $x$; and the power setting $\beta$ versus the distance $x$.

From Tables 3–5 and Figs. 3–5, the following conclusions can be inferred with reference to strong-to-severe windshears.

In Scheme (S1), the touchdown requirements can be satisfied for relatively low initial altitudes, while they cannot be satisfied for relatively high initial altitudes; the major inconvenient is excess of velocity at touchdown.

In Scheme (S2), the touchdown requirements cannot be satisfied, regardless of the initial altitude; the major inconvenient is defect of horizontal distance at touchdown.

In Scheme (S3), the touchdown requirements can be satisfied, and the optimal trajectories exhibit the following characteristics:

(i) the angle of attack has an initial decrease, which is followed by a gradual, sustained increase; the largest value of the angle of attack is attained near the end of the shear; in the aftershear region, the angle of attack decreases gradually;

(ii) initially, the power setting increases at a constant time rate until maximum power setting is reached; then, maximum power setting is maintained in the shear region; in the aftershear region, the power setting decreases gradually;

(iii) the relative velocity decreases in the shear region and increases in the aftershear region; the point of minimum velocity occurs at the end of the shear;

(iv) depending on the windshear intensity and the initial altitude, the deviations of the flight trajectory from the nominal trajectory can be considerable in the shear region; however, these deviations become small in the aftershear region, and the optimal flight trajectory recovers the nominal trajectory.

**Remark.** If one compares abort landing with penetration landing, it is clear that the former is to be preferred if the windshear is encountered at higher altitudes (large values of $h_0$), while the latter is to be preferred if the windshear is encountered at lower altitudes (low values of $h_0$). For low initial altitudes, the maximum power setting trajectory (OT1) and the control power setting trajectory (OT3) behave almost in the same way. This result is of interest and it might lead to considerable simplifications in the development of guidance schemes for low-altitude windshear encounter. For this type of encounter, the power setting is to be increased rapidly to the maximum value and is to be kept at the maximum value afterward; hence, the two-control guidance simplifies to a one-control guidance.

## 6. Comparison of Trajectories

In this section, we compare three trajectories: the optimal trajectory of the control power setting scheme (OT3); the fixed control trajectory (FCT), obtained by keeping constant both the angle of attack and the power setting; and the autoland trajectory (ALT), obtained by controlling the angle of attack via path inclination signals and controlling the power setting via velocity signals. The comparison is done in terms of the ability to meet the path inclination, velocity, and distance requirements at touchdown.

For the fixed control trajectory (FCT), the angle of attack and the power setting are given by

$$\alpha = \alpha_0, \tag{39a}$$

$$\beta = \beta_0, \tag{39b}$$

where $\alpha_0, \beta_0$ denote prewindshear values.

For the autoland trajectory (ALT), the angle of attack and the power setting are given by the following feedback control laws:

$$\alpha - \tilde{\alpha}(V) = -K_1[\gamma_e - \tilde{\gamma}_e(h)], \tag{40a}$$

$$\tilde{\alpha} = \tilde{\alpha}(V) \text{ as in Ref. 14}, \tag{40b}$$

$$\tilde{\gamma}_e = \gamma_{e0}, \qquad \text{if } h \geq h_f, \tag{40c}$$

$$\tilde{\gamma}_e = \gamma_{e\tau} + (\gamma_{e0} - \gamma_{e\tau})h/h_f, \qquad \text{if } h \leq h_f, \tag{40d}$$

$$\alpha \leq \alpha_*, \qquad -\dot{\alpha}_* \leq \dot{\alpha} \leq \dot{\alpha}_*, \tag{40e}$$

and

$$\beta - \beta_0 = -K_2(V - V_0), \qquad K_2 = (1 - \beta_0)/(V_0 - V_{\tau l}), \tag{41a}$$

$$\beta_* \leq \beta \leq 1, \qquad -\dot{\beta}_* \leq \dot{\beta} \leq \dot{\beta}_*. \tag{41b}$$

In the above relations, $\tilde{\alpha}(V)$ is the nominal angle of attack, whose conception is described in Ref. 14; $\tilde{\gamma}_e(h)$ is the nominal absolute path inclination; $\gamma_{e0}$ is the absolute path inclination at the initial point; $\gamma_{e\tau}$ is the absolute path inclination at touchdown; and $h_f$ is the altitude at the end of the approach path/beginning of the flare path. The constants appearing in Eqs. (40)–(41) have the following values:

$$\gamma_{e0} = -3.0 \text{ deg}, \qquad \gamma_{e\tau} = -0.5 \text{ deg}, \qquad h_f = 50 \text{ ft}, \tag{42a}$$

$$\beta_0 = 0.3330, \qquad V_0 = 239.7 \text{ ft sec}^{-1}, \qquad V_{\tau l} = 189.0 \text{ ft sec}^{-1}, \tag{42b}$$

and the gain coefficients appearing in Eqs. (40)–(41) have the following values:

$$K_1 = 5, \qquad K_2 = 0.01316 \text{ ft}^{-1} \text{ sec}. \tag{43}$$

Note that, in the feedback control law (40a), the change of the angle of attack from its nominal value is proportional to the change of the absolute path inclination from its nominal value. Also note that, in the feedback control law (41a), the change of the power setting from its nominal value is proportional to the change of the relative velocity from its nominal value; in addition, the gain coefficient $K_2$ is such that maximum power setting is achieved when the relative velocity equals the lower bound $V_{\tau l}$; hence in (41a),

$$\beta = 1, \qquad \text{if } V = V_{\tau l}. \tag{44}$$

Several combinations of initial altitudes and windshear intensities were considered, specifically:

$$h_0 = 200, 600, 1000 \text{ ft}, \tag{45a}$$

$$\Delta W_x = 100, 120, 140 \text{ ft sec}^{-1}. \tag{45b}$$

The numerical results are shown in Figs. 6–8.

Figure 6 refers to $h_0 = 600$ ft and $\Delta W_x = 100$ ft sec$^{-1}$; Fig. 7 refers to $h_0 = 600$ ft and $\Delta W_x = 120$ ft sec$^{-1}$; and Fig. 8 refers to $h_0 = 600$ ft and $\Delta W_x = 140$ ft sec$^{-1}$. The following trajectories are shown in Figs. 6–8: the optimal trajectory for control power setting (OT3); the fixed control trajectory (FCT): the autoland trajectory (ALT); and the nominal trajectory (NT). Each figure includes four parts: the altitude $h$ versus the distance $x$; the relative velocity $V$ versus the distance $x$; the angle of attack $\alpha$ versus the

distance $x$; and the power setting $\beta$ versus the distance $x$. From Figs. 6–8, the following conclusions can be inferred.

(i) The fixed control trajectory (FCT) is unable to meet the specified touchdown requirements; this statement holds regardless of the windshear intensity and the initial altitude.

(ii) The autoland trajectory (ALT) is able to meet the specified touchdown requirements for weak-to-moderate windshears, but not for strong-to-severe windshears; for severe windshears, an undesirable characteristic of the autoland trajectory is that the point of minimum velocity occurs before the end of the shear; the velocity increase in the windshear region is coupled with severe altitude loss, occasionally resulting in a crash.

(iii) The optimal trajectory of the control power setting scheme (OT3) is able to meet the specified touchdown requirements for all the combinations of initial altitudes and windshear intensities considered here.

(iv) It is felt that guidance schemes based on the properties of the optimal trajectory of the control power setting scheme (OT3) should prove to be superior to alternative guidance schemes, such as the fixed control guidance scheme and the autoland guidance scheme.

## 7. Conclusions

This paper is concerned with optimal flight trajectories in the presence of windshear. The penetration landing problem is considered with reference to flight in a vertical plane, governed by either one control (the angle of attack, if the power setting is predetermined) or two controls (the angle of attack and the power setting). Inequality constraints are imposed on the angle of attack, the power setting, and their time derivatives.

The performance index being minimized measures the deviation of the flight trajectory from the nominal trajectory. In turn, the nominal trajectory includes two parts: the approach part, in which the slope is constant; and the flare part, in which the slope is a linear function of the horizontal distance. In the optimization process, the time is free; the absolute path inclination at touchdown is specified; the touchdown velocity is subject to upper and lower bounds; and the touchdown distance is subject to upper and lower bounds.

Three power setting schemes are investigated: (S1) maximum power setting; (S2) constant power setting; and (S3) control power setting. In Scheme (S1), it is assumed that, immediately after the windshear onset, the power setting is increased at a constant time rate until maximum power setting is reached; afterward, the power setting is held constant; in this scheme, the only control is the angle of attack. In Scheme (S2), it is assumed

that the power setting is held at a constant value, equal to the prewindshear value; in this scheme, the only control is the angle of attack. In Scheme (S3), the power setting is regarded as a control, just as the angle of attack.

Under the above conditions, the optimal control problem is solved by means of the primal sequential gradient-restoration algorithm (PSGRA). Numerical results are obtained for several combinations of windshear intensities and initial altitudes. The main conclusions are given below with reference to strong-to-severe windshears.

In Scheme (S1), the touchdown requirements can be satisfied for relatively low initial altitudes, while they cannot be satisfied for relatively high initial altitudes; the major inconvenient is excess of velocity at touchdown.

In Scheme (S2), the touchdown requirements cannot be satisfied, regardless of the initial altitude; the major inconvenient is defect of horizontal distance at touchdown.

In Scheme (S3), the touchdown requirements can be satisfied, and the optimal trajectories exhibit the following characteristics:

(i) the angle of attack has an initial decrease, which is followed by a gradual, sustained increase; the largest value of the angle of attack is attained near the end of the shear; in the aftershear region, the angle of attack decreases gradually;

(ii) initially, the power setting increases rapidly until maximum power setting is reached; then, maximum power setting is maintained in the shear region; in the aftershear region, the power setting decreases gradually;

(iii) the relative velocity decreases in the shear region and increases in the aftershear region; the point of minimum velocity occurs at the end of the shear;

(iv) depending on the windshear intensity and the initial altitude, the deviations of the flight trajectory from the nominal trajectory can be considerable in the shear region; however, these deviations become small in the aftershear region, and the optimal flight trajectory recovers the nominal trajectory.

A comparison is shown between the optimal trajectories of Scheme (S3) and the trajectories arising from alternative guidance schemes, such as fixed controls (fixed angle of attack, coupled with fixed power setting) and autoland (angle of attack controlled via path inclination signals, coupled with power setting controlled via velocity signals). The superiority of the optimal trajectories of Scheme (S3) is shown in terms of the ability to meet the path inclination, velocity, and distance requirements at touchdown. Therefore, it is felt that guidance schemes based on the properties of the optimal trajectories of Scheme (S3) should prove to be superior to alternative

guidance schemes, such as the fixed control guidance scheme and the autoland guidance scheme.

## References


1. FUJITA, T. T., *The Downburst*, Department of Geophysical Sciences, University of Chicago, Chicago, Illinois, 1985.
2. ANONYMOUS, N. N., *Aircraft Accident Report: Pan American World Airways, Clipper 759, Boeing 727-235, N4737, New Orleans International Airport, Kenner, Louisiana, July 9, 1982*, Report No. NTSB-AAR-8302, National Transportation Safety Board, Washington, DC, 1983.
3. ANONYMOUS, N. N., *Aircraft Accident Report: Delta Air Lines, Lockheed L-1011-30851, N726DA, Dallas-Fort Worth International Airport, Texas, August 2, 1985*, Report No. NTSB-AAR-8065, National Transportation Safety Board, Washington, DC, 1986.
4. FUJITA, T. T., *DFW Microburst*, Department of Geophysical Sciences, University of Chicago, Chicago, Illinois, 1986.
5. GORNEY, J. L., *An Analysis of the Delta 191 Windshear Accident*, Paper No. AIAA-87-0626, AIAA 25th Aerospace Sciences Meeting, Reno, Nevada, 1987.
6. FROST, W., *Flight in Low-Level Windshear*, NASA, Contractor Report No. 3678, 1983.
7. PSIAKI, M. L., and STENGEL, R. F., *Analysis of Aircraft Control Strategies for Microburst Encounter*, Paper No. AIAA-84-0238, AIAA 22nd Aerospace Sciences Meeting, Reno, Nevada, 1984.
8. PSIAKI, M. L., and STENGEL, R. F., *Optimal Flight Paths through Microburst Wind Profiles*, Journal of Aircraft, Vol. 23, No. 8, pp. 629–635, 1986.
9. CHU, P. Y., and BRYSON, A. E., JR., *Control of Aircraft Landing Approach in Windshear*, Paper No. AIAA-87-0632, AIAA 25th Aerospace Sciences Meeting, Reno, Nevada, 1987.
10. HAHN, K. U., *Take-Off and Landing in a Downburst*, Paper No. ICAS-86-562, 15th Congress of the International Council of the Aeronautical Sciences, London, England, 1986.
11. MIELE, A. WANG, T., and MELVIN, W. W., *Penetration Landing Guidance Trajectories in the Presence of Windshear*, Rice University, Aero-Astronautics Report No. 218, 1987.
12. MIELE, A., WANG, T., and MELVIN, W. W., *Optimal Take-Off Trajectories in the Presence of Windshear*, Journal of Optimization Theory and Applications, Vol. 49, No. 1, pp. 1–45, 1986.
13. MIELE, A., WANG, T., and MELVIN, W. W., *Guidance Strategies for Near-Optimum Take-Off Performance in a Windshear*, Journal of Optimization Theory and Applications, Vol. 50, No. 1, pp. 1–47, 1986.
14. MIELE, A., WANG, T., and MELVIN, W. W., *Optimization and Acceleration Guidance of Flight Trajectories in a Windshear*, Journal of Guidance, Control, and Dynamics, Vol. 10, No. 4, pp. 368–377, 1987.

15. MIELE, A., WANG, T., MELVIN, W. W., and BOWLES, R. L., *Gamma Guidance Schemes for Flight in a Windshear*, Journal of Guidance, Control, and Dynamics, Vol. 11, 1988 (to appear).
16. MIELE, A., WANG, T., MELVIN, W. W., and BOWLES, R. L. *Maximum Survival Capability of an Aircraft in a Severe Windshear*, Journal of Optimization Theory and Applications, Vol. 53, No. 2, pp. 181–217, 1987.
17. MIELE, A., WANG, T., and MELVIN, W. W., *Quasi-Steady Flight to Quasi-Steady Flight Transition in a Windshear: Trajectory Optimization and Guidance*, Journal of Optimization Theory and Applications, Vol. 54, No. 2, pp. 203–240, 1987.
18. MIELE, A., WANG, T., TZENG, C. Y., and MELVIN, W. W., *Transformation Techniques for Minimax Optimal Control Problems and Their Application to Optimal Flight Trajectories in a Windshear: Optimal Abort Landing Trajectories*, Paper No. IFAC-87-9221, IFAC 10th World Congress, Munich, Germany, 1987.
19. MIELE, A., WANG, T., TZENG, C. Y., and MELVIN, W. W., *Optimization and Guidance of Abort Landing Trajectories in a Windshear*, Paper No. AIAA-87-2341, AIAA Guidance, Navigation, and Control Conference, Monterey, California, 1987.
20. MIELE, A., WANG, T., and MELVIN, W. W., *Acceleration, Gamma, and Theta Guidance Schemes for Abort Landing Trajectories in the Presence of Windshear*, Rice University, Aero-Astronautics Report No. 223, 1987.
21. IVAN, M., *A Ring-Vortex Downburst Model for Flight Simulation*, Journal of Aircraft, Vol. 23, No. 3, pp. 232–236, 1986.
22. WINGROVE, R. C., and BACH, R. E., JR., *Severe Winds in the DFW Microburst Measured from Two Aircraft*, Paper No. AIAA-87-2340, AIAA Guidance, Navigation, and Control Conference, Monterey, California, 1987.
23. MIELE, A., and WANG, T., *Primal-Dual Properties of Sequential Gradient-Restoration Algorithms for Optimal Control Problems, Part 1, Basic Problem*, Integral Methods in Science and Engineering, Edited by F. R. Payne *et al.*, Hemisphere Publishing Corporation, Washington, DC, pp. 577–607, 1986.
24. MIELE, A., and WANG, T., *Primal-Dual Properties of Sequential Gradient-Restoration Algorithms for Optimal Control Problems, Part 2, General Problem*, Journal of Mathematical Analysis and Applications, Vol. 119, Nos. 1–2, pp. 21–54, 1986.

Table 1. Initial conditions.

| Quantity | $\lambda = 0.00$ | $\lambda = 1.00$ | $\lambda = 1.20$ | $\lambda = 1.40$ | Units |
|---|---|---|---|---|---|
| $V_0$ | 239.7 | 239.7 | 239.7 | 239.7 | ft sec$^{-1}$ |
| $\gamma_{e0}$ | −3.000 | −3.000 | −3.000 | −3.000 | deg |
| $\gamma_0$ | −3.000 | −2.375 | −2.249 | −2.124 | deg |
| $\alpha_0$ | 7.370 | 7.353 | 7.349 | 7.345 | deg |
| $\theta_0$ | 4.370 | 4.978 | 5.100 | 5.221 | deg |
| $\beta_0$ | 0.3330 | 0.3743 | 0.3825 | 0.3907 | — |

Table 2. Final conditions.

| Quantity | $h_0 = 200$ ft | $h_0 = 600$ ft | $h_0 = 1000$ ft | Units |
|---|---|---|---|---|
| $h_\tau$ | 0.0 | 0.0 | 0.0 | ft |
| $\gamma_{e\tau}$ | −0.5 | −0.5 | −0.5 | deg |
| $V_{\tau l}$ | 189.0 | 189.0 | 189.0 | ft sec$^{-1}$ |
| $V_{\tau u}$ | 290.3 | 290.3 | 290.3 | ft sec$^{-1}$ |
| $\tilde{V}_\tau$ | 239.7 | 239.7 | 239.7 | ft sec$^{-1}$ |
| $x_{\tau l}$ | 3498 | 11130 | 18763 | ft |
| $\chi_{\tau u}$ | 5498 | 13130 | 20763 | ft |
| $\tilde{x}_\tau$ | 4498 | 12130 | 19763 | ft |

Table 3. Numerical results for Problem (P1), maximum power setting [Scheme (S1)].

| $h_0$ (ft) | $\Delta W_x$ (ft sec$^{-1}$) | $\tau$ (sec) | $\gamma_{e\tau}$ (deg) | $V_\tau - \tilde{V}_\tau$ (ft sec$^{-1}$) | $x_\tau - \tilde{x}_\tau$ (ft) | $\lvert\Delta h\rvert_{\max}$ (ft) | $\lvert\Delta h\rvert_{\text{ave}}$ (ft) |
|---|---|---|---|---|---|---|---|
| 200 | 100 | 19.4 | −0.5 | −10.2 | 2.9 | 0.7 | 0.4 |
| 200 | 120 | 20.3 | −0.5 | −27.2 | 14.2 | 3.6 | 2.3 |
| 200 | 140 | 21.1 | −0.5 | −45.2 | 23.5 | 4.2 | 2.7 |
| 600 | 100 | 43.9 | −0.5 | 88.4 (*) | −6.0 | 5.4 | 3.0 |
| 600 | 120 | 46.3 | −0.5 | 73.2 (*) | −8.2 | 17.8 | 8.2 |
| 600 | 140 | 47.1 | −0.5 | 58.7 (*) | 30.8 | 120.5 | 70.1 |
| 1000 | 100 | 66.1 | −0.5 | 132.1 (*) | −37.2 | 85.5 | 40.4 |
| 1000 | 120 | 67.3 | −0.5 | 124.3 (*) | 92.2 | 218.2 | 116.6 |
| 1000 | 140 | 67.8 | −0.5 | 115.5 (*) | −40.5 | 366.6 | 195.5 |

(*) Asterisk denotes violation of touchdown inequality constraint.

Table 4. Numerical results for Problem (P2), constant power setting [Scheme (S2)].

| $h_0$ (ft) | $\Delta W_x$ (ft sec$^{-1}$) | $\tau$ (sec) | $\gamma_{e\tau}$ (deg) | $V_\tau - \tilde{V}_\tau$ (ft sec$^{-1}$) | $x_\tau - \tilde{x}_\tau$ (ft) | $\lvert\Delta h\rvert_{\max}$ (ft) | $\lvert\Delta h\rvert_{\text{ave}}$ (ft) |
|---|---|---|---|---|---|---|---|
| 200 | 100 | 13.8 | −0.5 | −56.4 (*) | −1825 (*) | 78.2 | 60.5 |
| 200 | 120 | 12.6 | −0.5 | −55.1 (*) | −2170 (*) | 92.8 | 75.7 |
| 200 | 140 | 11.8 | −0.5 | −54.1 (*) | −2428 (*) | 103.8 | 87.5 |
| 600 | 100 | 17.5 | −0.5 | −43.9 | −8503 (*) | 419.3 | 279.4 |
| 600 | 120 | 15.6 | −0.5 | −42.5 | −8979 (*) | 443.0 | 312.9 |
| 600 | 140 | 14.3 | −0.5 | −41.8 | −9350 (*) | 461.4 | 337.2 |
| 1000 | 100 | 22.0 | −0.5 | −32.4 | −15215 (*) | 769.0 | 462.1 |
| 1000 | 120 | 18.5 | −0.5 | −31.9 | −15930 (*) | 805.5 | 508.7 |
| 1000 | 140 | 16.7 | −0.5 | −32.8 | −16343 (*) | 826.9 | 557.7 |

(*) Asterisk denotes violation of touchdown inequality constraint.

Table 5. Numerical results for Problem (P3), control power setting [Scheme (S3)].

| $h_0$ (ft) | $\Delta W_x$ (ft sec$^{-1}$) | $\tau$ (sec) | $\gamma_{e\tau}$ (deg) | $V_t - \tilde{V}_\tau$ (ft sec$^{-1}$) | $x_\tau - \tilde{x}_\tau$ (ft) | $\lvert\Delta h\rvert_{\max}$ (ft) | $\lvert\Delta h\rvert_{\text{ave}}$ (ft) |
|---|---|---|---|---|---|---|---|
| 200 | 100 | 21.5 | −0.5 | −35.4 | 47.1 | 0.6 | 0.3 |
| 200 | 120 | 21.6 | −0.5 | −37.3 | 111.4 | 1.3 | 0.6 |
| 200 | 140 | 21.9 | −0.5 | −46.4 | 150.2 | 1.7 | 0.9 |
| 600 | 100 | 47.8 | −0.5 | 7.6 | −551.9 | 13.7 | 6.9 |
| 600 | 120 | 46.5 | −0.5 | 7.6 | −712.3 | 24.3 | 13.3 |
| 600 | 140 | 49.8 | −0.5 | −26.6 | −207.2 | 109.9 | 61.6 |
| 1000 | 100 | 69.6 | −0.5 | 19.7 | −839.4 | 113.6 | 52.3 |
| 1000 | 120 | 72.0 | −0.5 | 13.0 | −795.2 | 212.8 | 108.1 |
| 1000 | 140 | 77.4 | −0.5 | 5.8 | −388.4 | 358.9 | 175.9 |

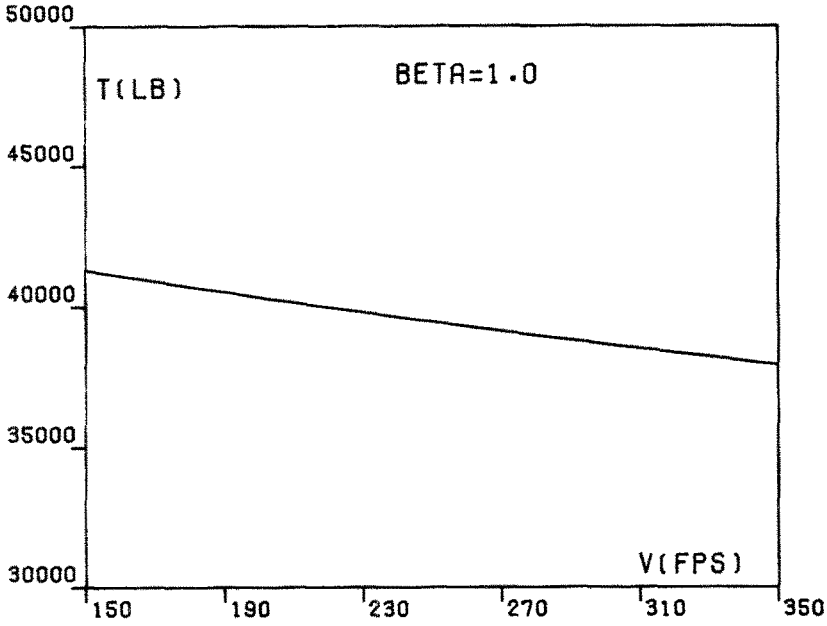


Fig. 1A. Thrust $T_*$ versus velocity $V$ for the Boeing B-727 aircraft powered by three JT8D-17 turbofan engines (maximum power setting, sea-level altitude, ambient temperature = 100 deg Fahrenheit).

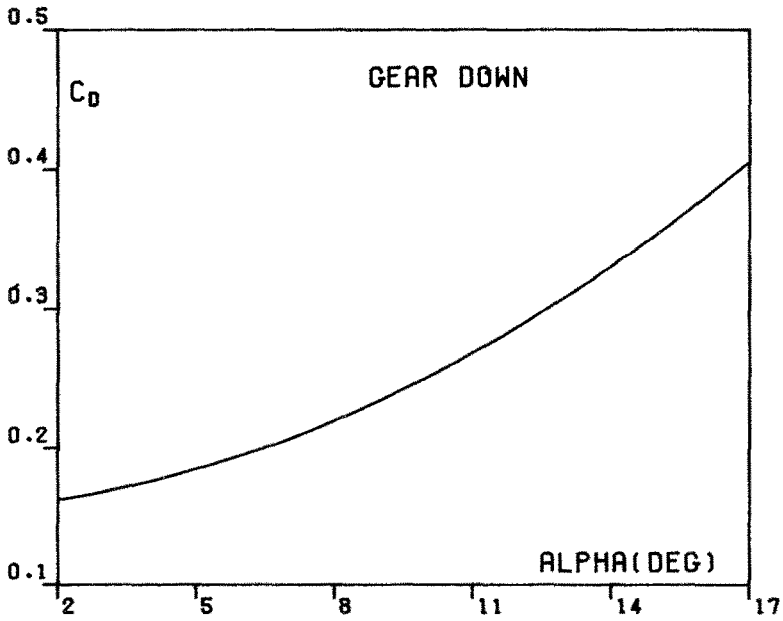


Fig. 1B. Drag coefficient $C_D$ versus angle of attack $\alpha$ for the Boeing B-727 aircraft (gear down, flap setting $\delta_F = 30$ deg).

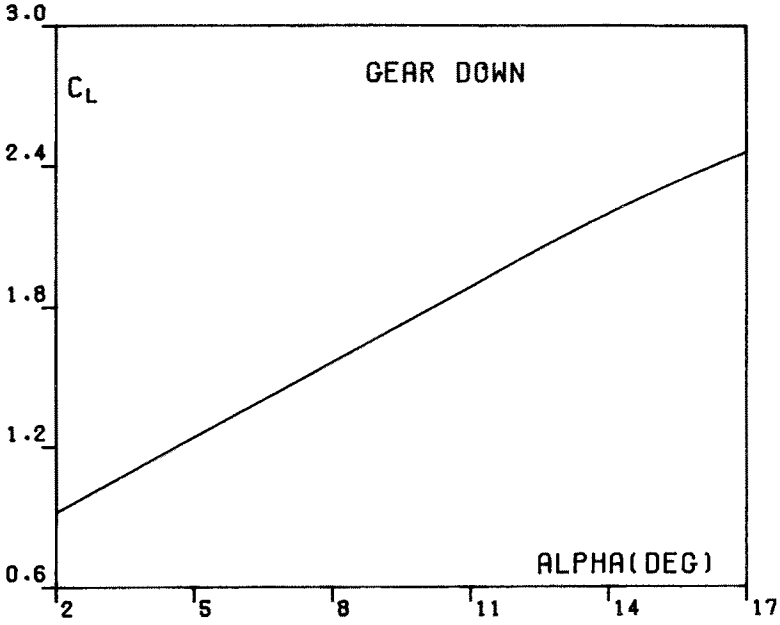


Fig. 1C. Lift coefficient $C_L$ versus angle of attack $\alpha$ for the Boeing B-727 aircraft (gear down, flap setting $\delta_F = 30$ deg).

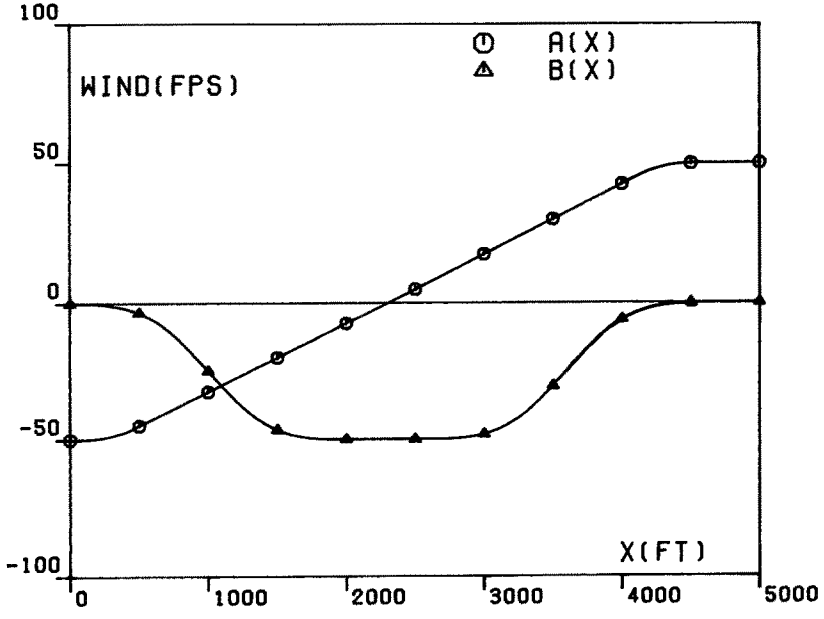


Fig. 2. Horizontal wind function $A(x)$ and vertical wind function $B(x)$.

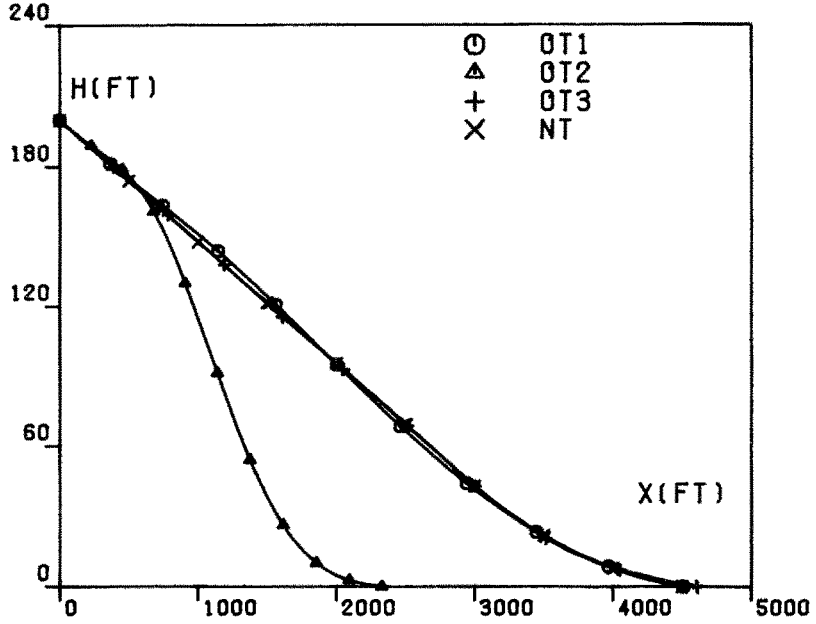


Fig. 3A. Optimal trajectories, $h_0 = 200$ ft, $\Delta W_x = 120$ ft sec$^{-1}$: altitude $h$ versus distance $x$.

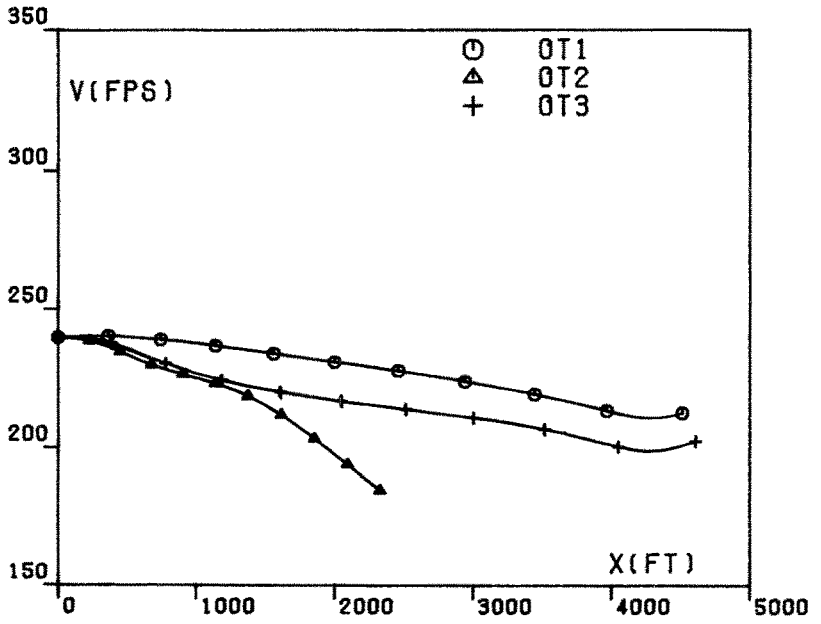


Fig. 3B. Optimal trajectories, $h_0 = 200$ ft, $\Delta W_x = 120$ ft sec$^{-1}$: relative velocity $V$ versus distance $x$.

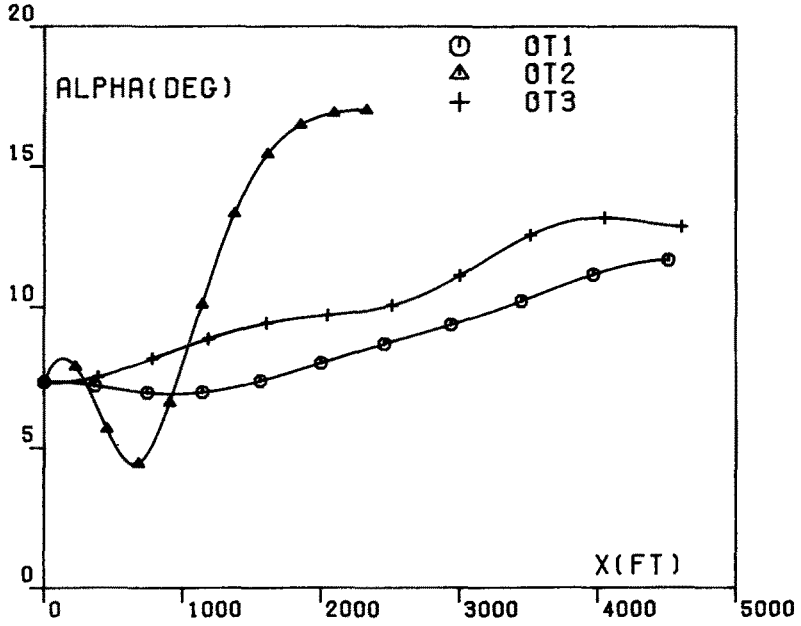


Fig. 3C. Optimal trajectories, $h_0 = 200$ ft, $\Delta W_x = 120$ ft sec$^{-1}$: angle of attack $\alpha$ versus distance $x$.

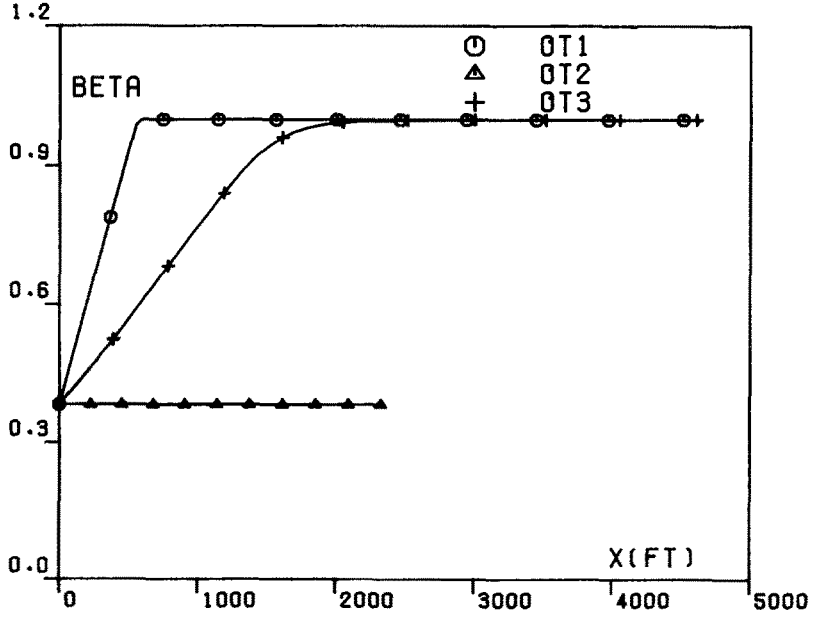


Fig. 3D. Optimal trajectories, $h_0 = 200$ ft, $\Delta W_x = 120$ ft sec$^{-1}$: power setting $\beta$ versus distance $x$.

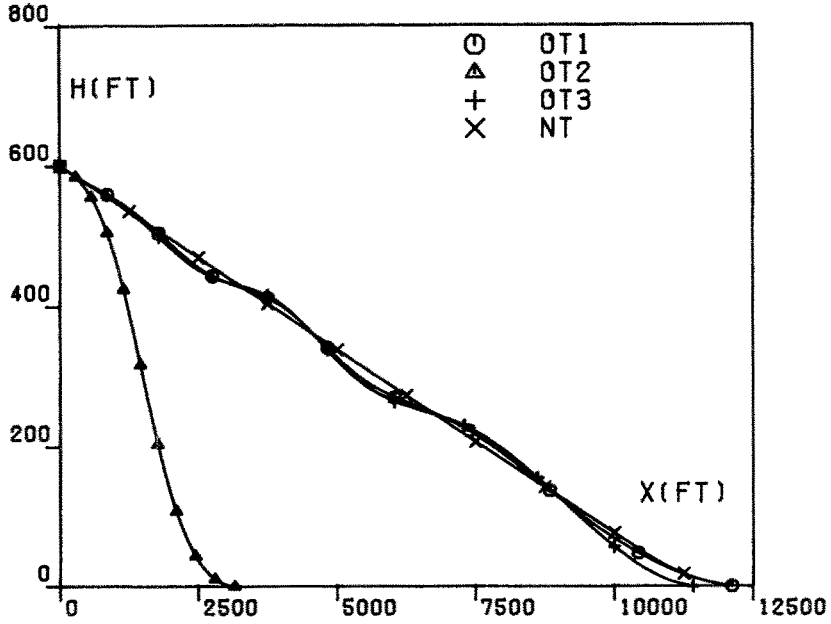


Fig. 4A. Optimal trajectories, $h_0 = 600$ ft, $\Delta W_x = 120$ ft sec$^{-1}$: altitude $h$ versus distance $x$.

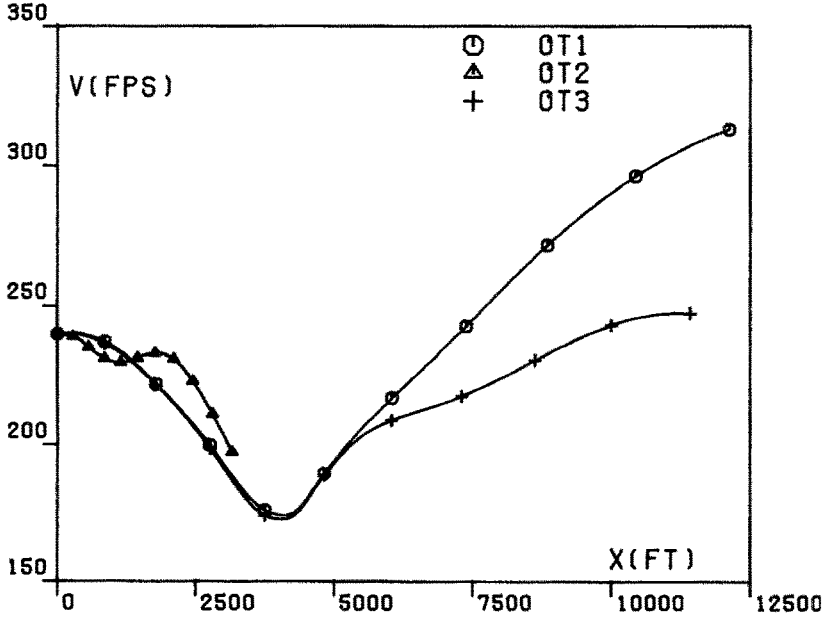


Fig. 4B. Optimal trajectories, $h_0 = 600$ ft, $\Delta W_x = 120$ ft sec$^{-1}$: relative velocity $V$ versus distance $x$.

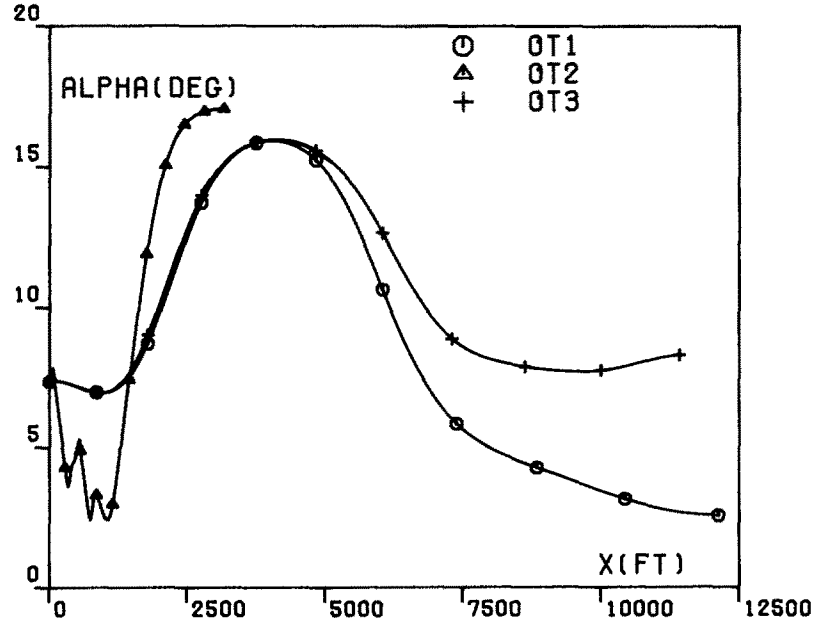


Fig. 4C. Optimal trajectories, $h_0 = 600$ ft, $\Delta W_x = 120$ ft sec$^{-1}$: angle of attack $\alpha$ versus distance $x$.

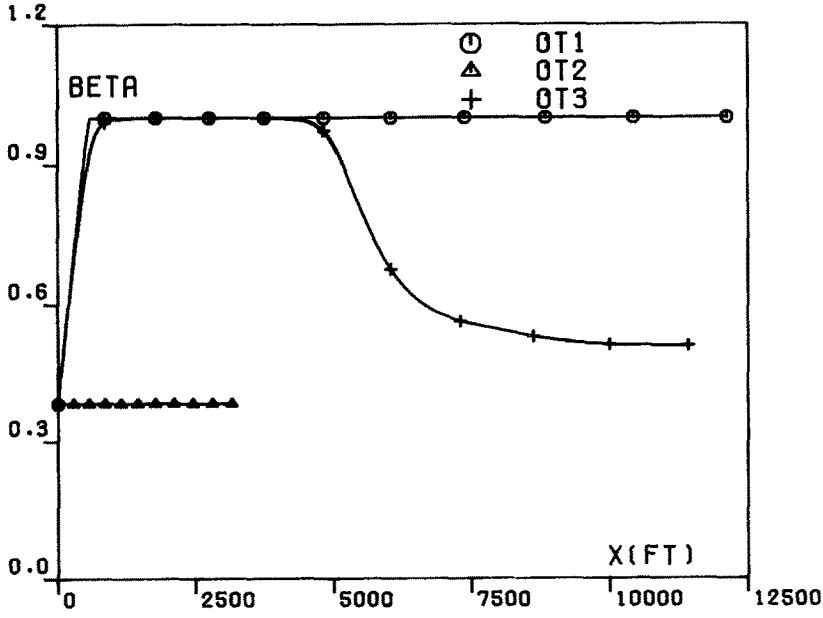


Fig. 4D. Optimal trajectories, $h_0 = 600$ ft, $\Delta W_x = 120$ ft sec$^{-1}$: power setting $\beta$ versus distance $x$.

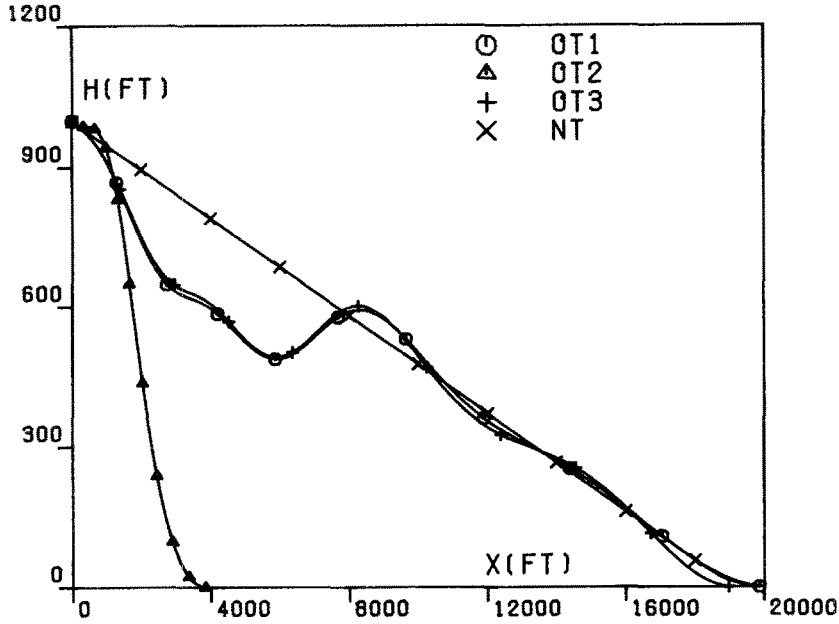


Fig. 5A. Optimal trajectories, $h_0 = 1000$ ft, $\Delta W_x = 120$ ft sec$^{-1}$: altitude $h$ versus distance $x$.

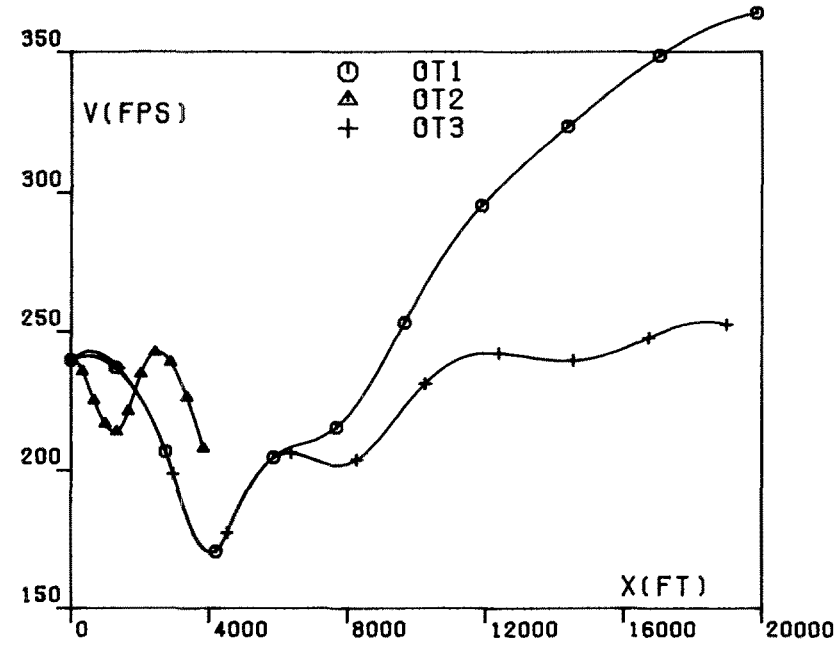


Fig. 5B. Optimal trajectories, $h_0 = 1000$ ft, $\Delta W_x = 120$ ft sec$^{-1}$: relative velocity $V$ versus distance $x$.

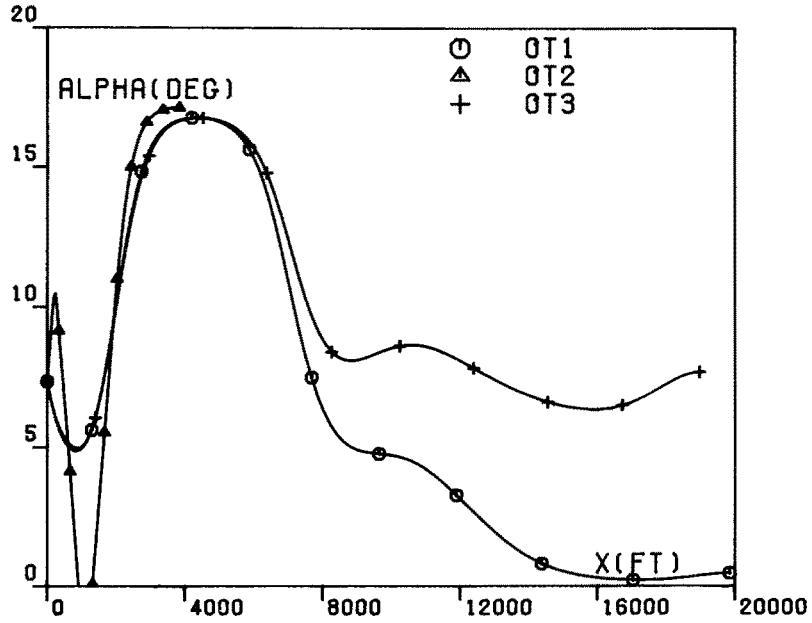


Fig. 5C. Optimal trajectories, $h_0 = 1000$ ft, $\Delta W_x = 120$ ft sec$^{-1}$: angle of attack $\alpha$ versus distance $x$.

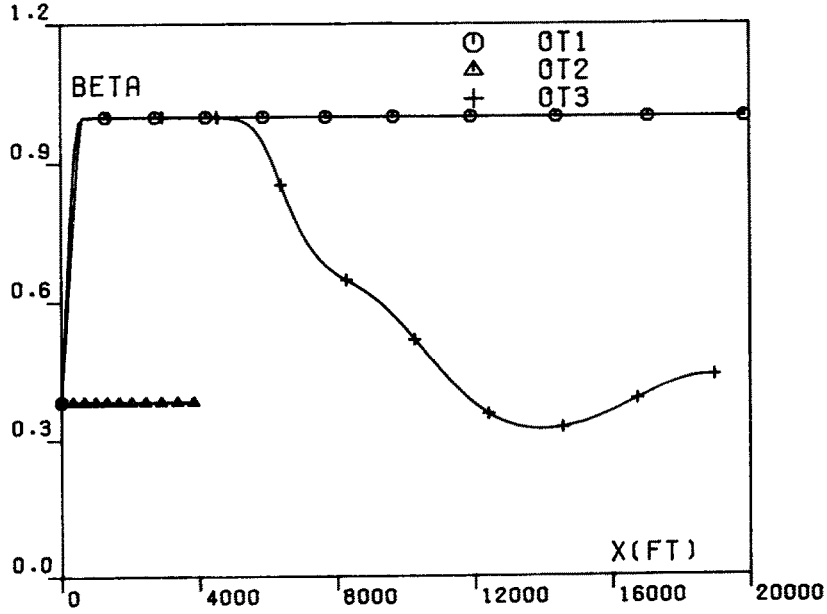


Fig. 5D. Optimal trajectories, $h_0 = 1000$ ft, $\Delta W_x = 120$ ft sec$^{-1}$: power setting $\beta$ versus distance $x$.

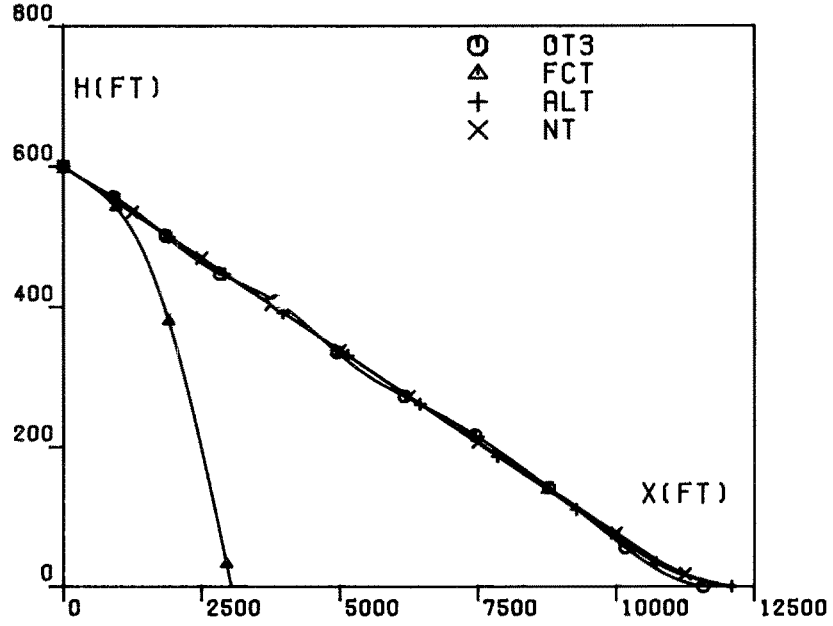


Fig. 6A. Comparison trajectories, $h_0 = 600$ ft, $\Delta W_x = 100$ ft sec$^{-1}$: altitude $h$ versus distance $x$.

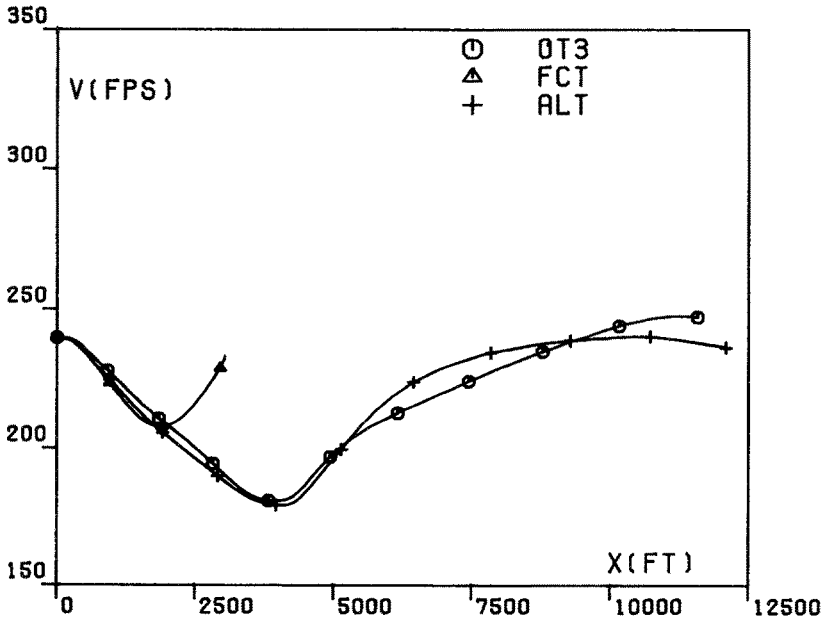


Fig. 6B. Comparison trajectories, $h_0 = 600$ ft, $\Delta W_x = 100$ ft sec$^{-1}$: relative velocity $V$ versus distance $x$.

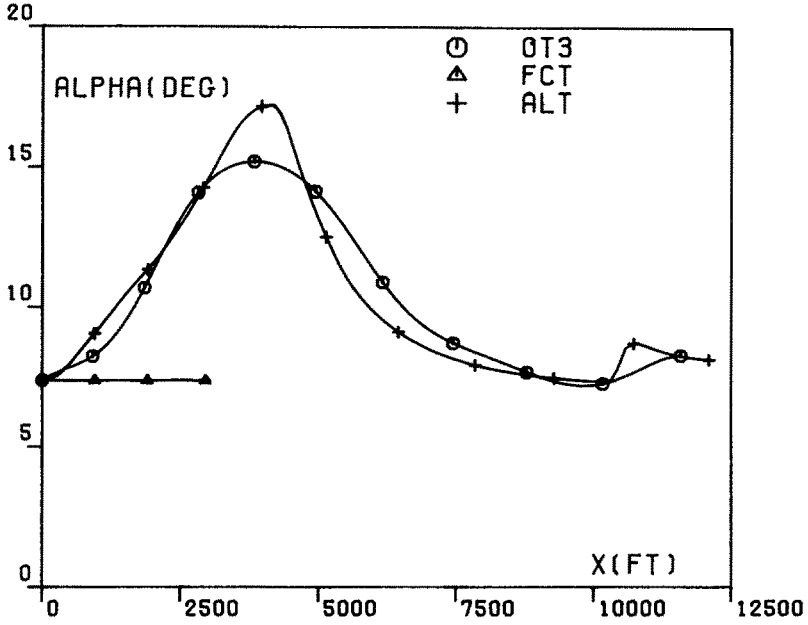


Fig. 6C. Comparison trajectories, $h_0 = 600$ ft, $\Delta W_x = 100$ ft sec$^{-1}$: angle of attack $\alpha$ versus distance $x$.

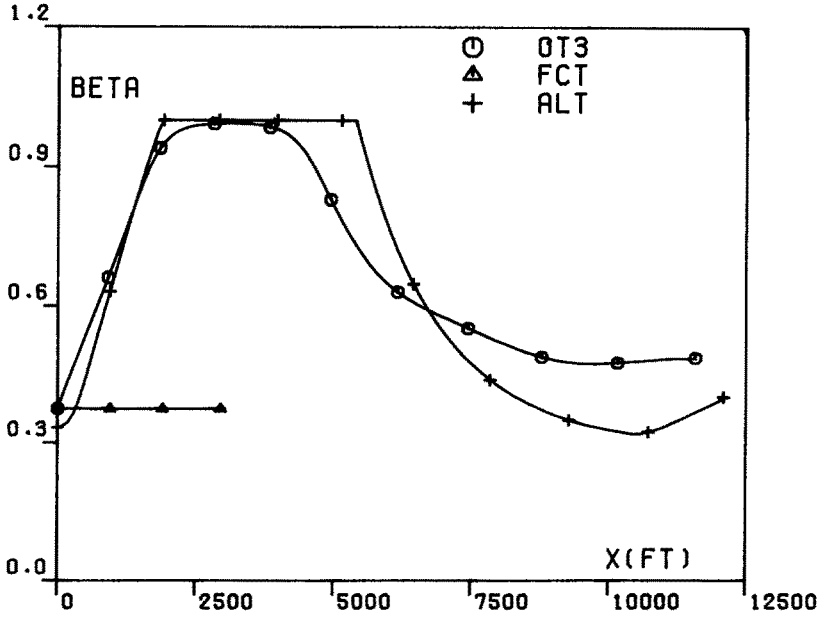


Fig. 6D. Comparison trajectories, $h_0 = 600$ ft, $\Delta W_x = 100$ ft sec$^{-1}$: power setting $\beta$ versus distance $x$.

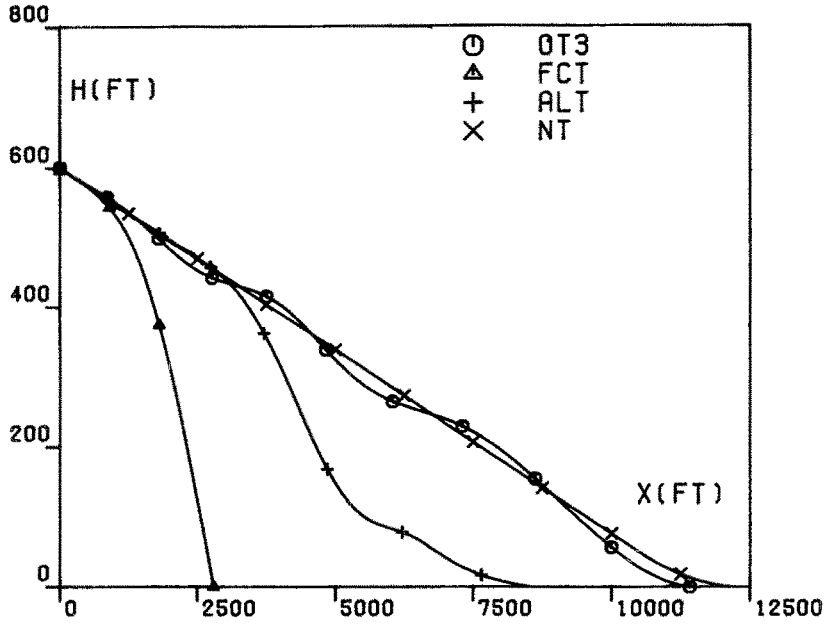


Fig. 7A. Comparison trajectories, $h_0 = 600$ ft, $\Delta W_x = 120$ ft sec$^{-1}$: altitude $h$ versus distance $x$.

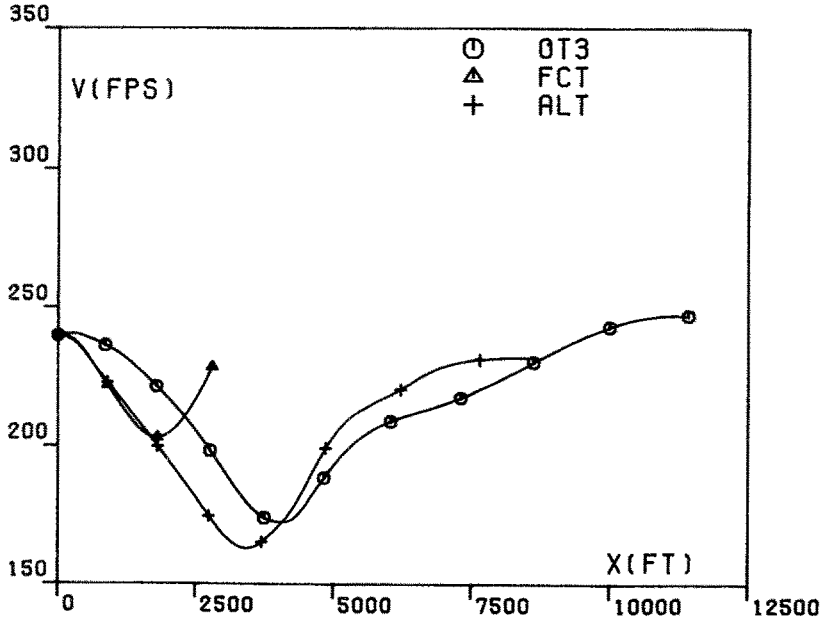


Fig. 7B. Comparison trajectories, $h_0 = 600$ ft, $\Delta W_x = 120$ ft sec$^{-1}$: relative velocity $V$ versus distance $x$.

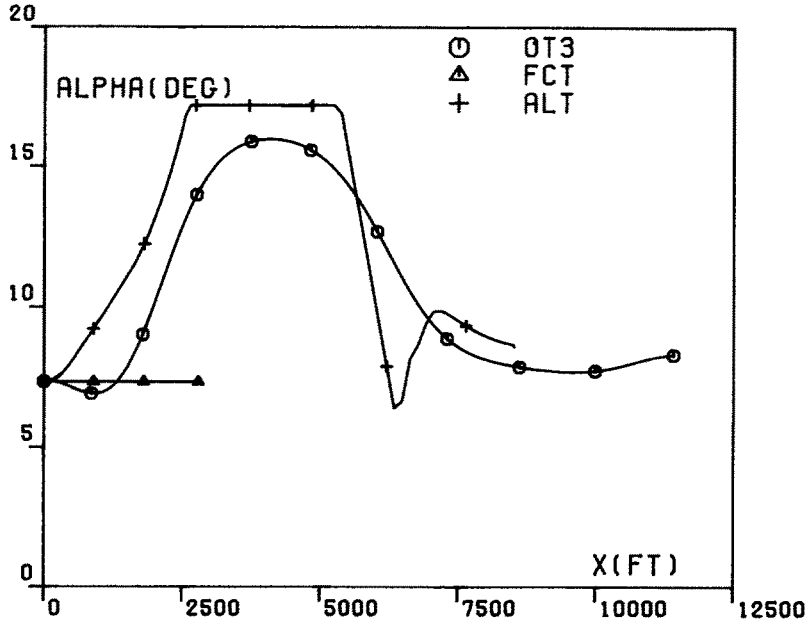


Fig. 7C. Comparison trajectories, $h_0 = 600$ ft, $\Delta W_x = 120$ ft sec$^{-1}$: angle of attack $\alpha$ versus distance $x$.

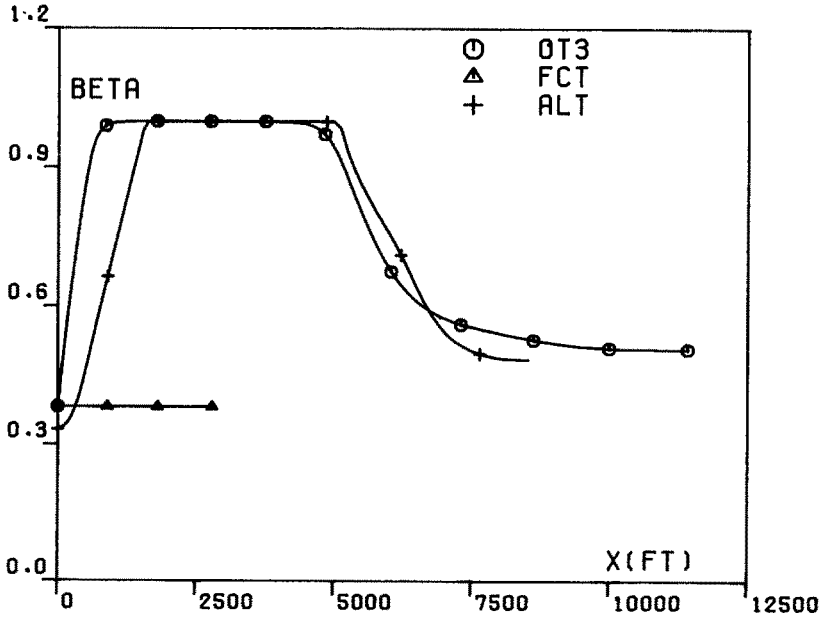


Fig. 7D. Comparison trajectories, $h_0 = 600$ ft, $\Delta W_x = 120$ ft sec$^{-1}$: power setting $\beta$ versus distance $x$.

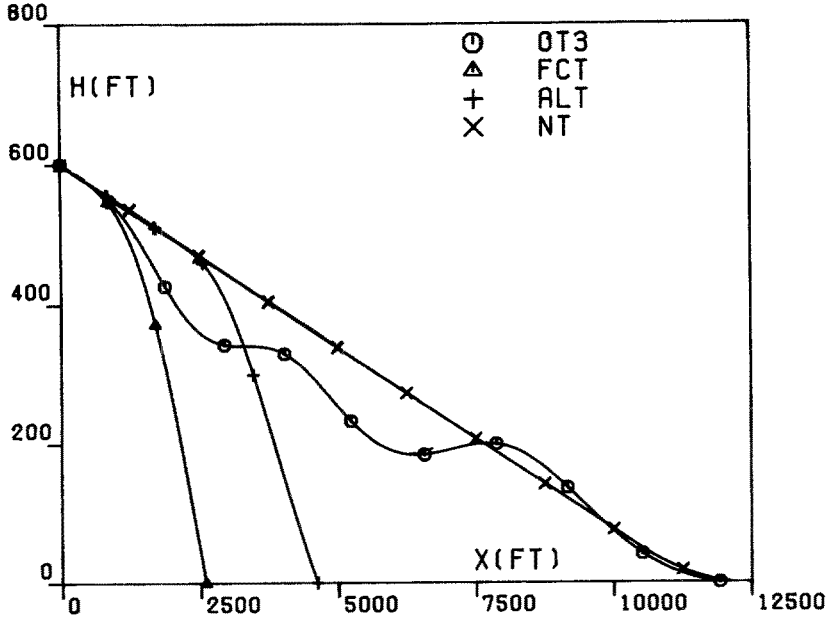


Fig. 8A. Comparison trajectories, $h_0 = 600$ ft, $\Delta W_x = 140$ ft sec$^{-1}$: altitude $h$ versus distance $x$.

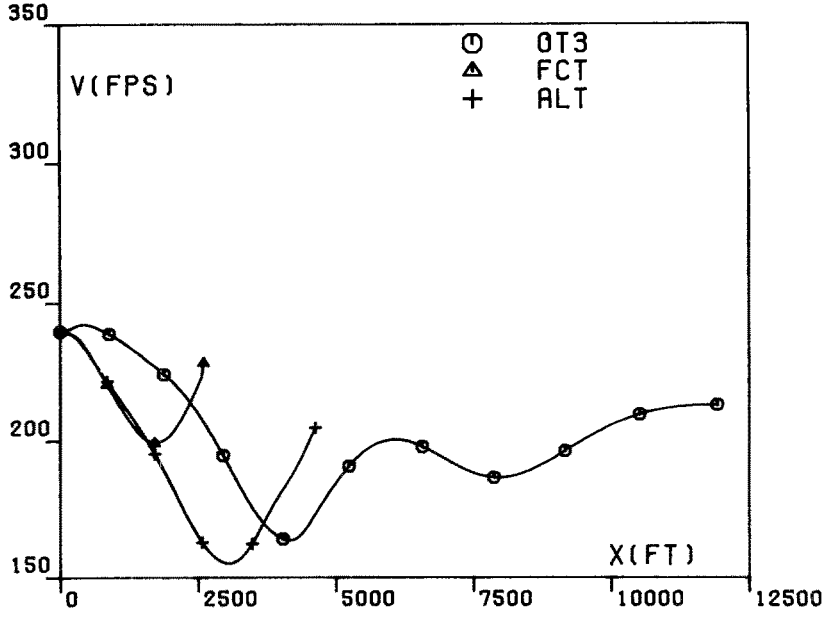


Fig. 8B. Comparison trajectories, $h_0 = 600$ ft, $\Delta W_x = 140$ ft sec$^{-1}$: relative velocity $V$ versus distance $x$.

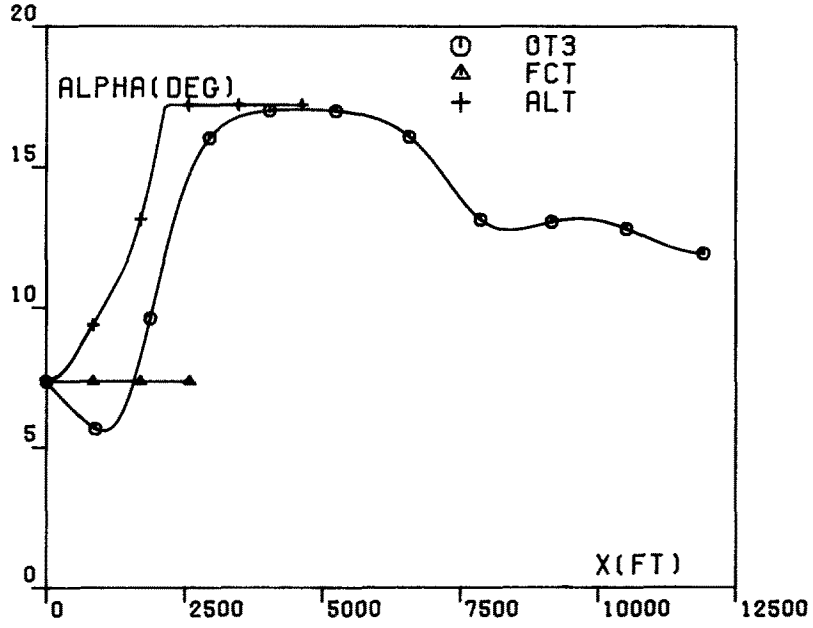


Fig. 8C. Comparison trajectories, $h_0 = 600$ ft, $\Delta W_x = 140$ ft sec$^{-1}$: angle of attack $\alpha$ versus distance $x$.

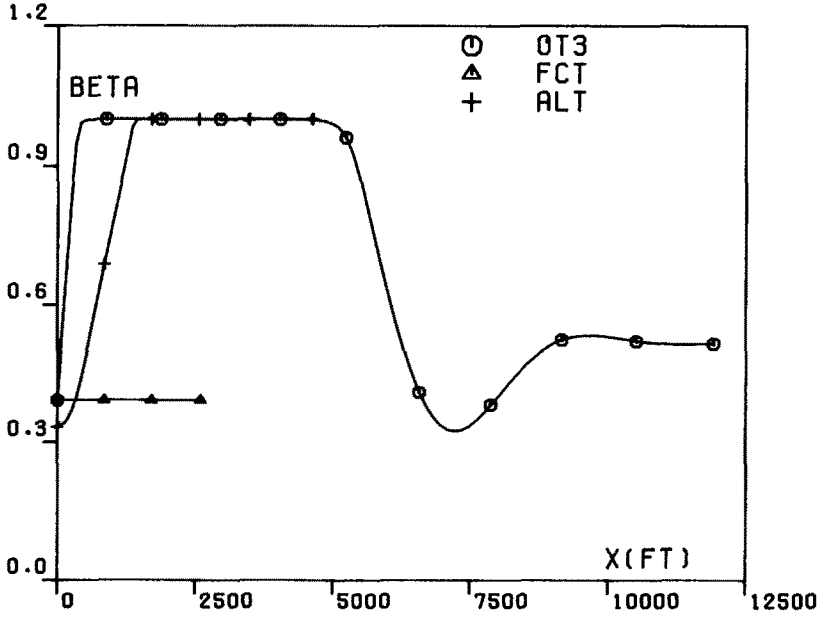


Fig. 8D. Comparison trajectories, $h_0 = 600$ ft, $\Delta W_x = 140$ ft sec$^{-1}$: power setting $\beta$ versus distance $x$.